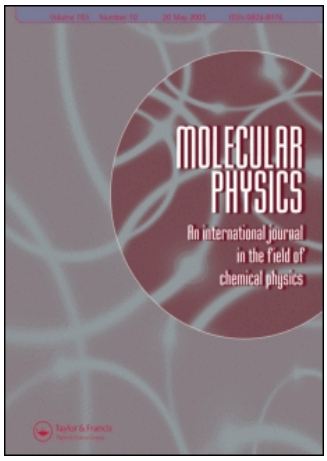

Molecular Physics
An International Journal in the Field of Chemical Physics
Publication details, including instructions for authors and subscription information:
http://www.informaworld.com/smpp/title~content=t713395160

Toward a precise determination of the acceptor switching splitting in the water dimer

To cite this Article: Harker, H. A., Keutsch, F. N., Leforestier, C., Scribano, Y., Han, J.-X. and Saykally, R. J. , 'Toward a precise determination of the acceptor switching splitting in the water dimer', Molecular Physics, 105:5, 497 - 512
To link to this article: DOI: 10.1080/00268970601063812
URL: http://dx.doi.org/10.1080/00268970601063812

Molecular Physics, Vol. 105, Nos. 5–7, 10 March–10 April 2007, 497–512

Toward a precise determination of the acceptor switching splitting in the water dimer

H. A. HARKER†, F. N. KEUTSCH‡, C. LEFORESTIER§, Y. SCRIBANO§, J.-X. HAN† and R. J. SAYKALLY*†

†University of California, USA
‡University of Wisconsin, USA
§Université de Montpellier II, France

(*Received 8 September 2006; in final form 29 September 2006*)

Precise measurement of all tunneling splittings in the ground vibrational state of the water dimer is essential for a complete and rigorous determination of the intermolecular potential energy surface. Here, accurate experimentally determined rotational constants and tunneling splittings were combined with estimates of the ground state acceptor switching (*AS*) splittings for both $(H_2O)_2$ and $(D_2O)_2$ in order to exactly predict the fingerprints of the weakly allowed $E_2 \leftrightarrow E_1$ transitions and to approximately predict their absolute frequencies. While these transitions are predicted to be quite weak, current technology guided by the now fairly complete water dimer data should permit their observation. The measurement of these weak transitions would permit the direct determination of *AS* splittings, which has so far eluded experiments.

1. Introduction

Spectroscopic studies of the intermolecular vibrations of small water clusters have produced highly detailed structural and dynamical information that has permitted the determination of a new generation of potential energy surfaces (PES) for water [1]. Studies of the water dimer are of particular significance in that 2-body forces alone account for ~75% of the cohesive energy in small water clusters and presumably in the liquid [2]. Moreover, if the induction interaction is properly described, a dimer potential will also accurately describe the leading many-body terms [3]. The primarily 2-body nature along with the rapid convergence of these non-additive terms provides the basis for constructing accurate PES for larger water clusters as well as for bulk water from 'spectroscopic' dimer potentials. Hence, it is crucial to seek a 'perfect' dimer Intermolecular Potential Energy Surface (IPS), while the spectroscopic data for trimers and larger clusters can serve to refine the many-body interactions [1].

Several dimer PESs of near-spectroscopic accuracy have recently been determined through this combination of experimental and *ab initio* data – VRT(ASP-W)I, II, and III, [4] SAPT-5st, [5] and MCY-5f [6]. While these potentials represent major advances toward the determination of an accurate 'first principles' model for water, it is nevertheless clear that some essential experimental data for the dimer are still missing. Leforestier *et al*. showed that the 'tuning' of the SAPT-5s potential in order to reproduce experimental cluster data 'mimics the missing key ingredient of the actual pair potential, viz., flexibility of the monomers' [6]. Indeed, the SAPT-5st potential is the result of adjusting to only one experimental parameter, the sum of the ground state acceptor switching (*AS*) splittings $AS^{(0)} + AS^{(1)}$. A direct measurement of *individual AS* splittings (only sums and differences are currently available) in both the ground and vibrationally excited states of the water dimer would consequently provide both a rigorous test and a new experimental constraint for the effects of monomer flexibility.

An estimate of the individual *AS* splittings in $(D_2O)_2$ has already been extracted by Paul *et al*. [7] from IR cavity ringdown spectroscopy experiments. The splittings were determined indirectly by fitting ground- and excited-state acceptor tunneling splitting patterns to

*Corresponding author. Email: saykally@calmail.berkeley.edu

Molecular Physics
ISSN 0026–8976 print/ISSN 1362–3028 online © 2007 Taylor & Francis
http://www.tandf.co.uk/journals
DOI: 10.1080/00268970601063812

cosine functions that accurately reproduced the energy level diagram for the hydrogen-bond-acceptor antisymmetric stretch. Such periodicity is expected in the case of Coriolis coupling between the angular momentum generated by the tunneling motion and that from the overall rotation of the cluster. Nonetheless, it was necessary to assume identical (global inversion aside) splitting patterns for both the ground- and excited-states of the hydrogen-bond-acceptor antisymmetric stretching vibration in order to arrive at such an estimate of the *AS* splittings. Here, we describe a means with which to precisely determine the $(D_2O)_2$ and $(H_2O)_2$ ground state *AS* splittings that remain only slightly beyond the reach of current experimental capability.

2. Background

Previous studies indicate that the water dimer is a highly nonrigid, near-prolate top (figure 1) that simultaneously undergoes three large amplitude tunneling motions [8–15]. Tunneling occurs among eight degenerate minima on the 12D IPS (6D for rigid potentials) via three low barrier pathways [16, 17]. A correlation diagram for the $K_a = 0$, $J = 0$ ground vibration–rotation–tunneling (VRT) energy levels of the water dimer (figure 2) shows the splittings of the rovibrational levels that result from these tunneling motions [9, 13, 15]. The magnitude of the splitting or shift of the VRT states is inversely related to the tunneling barriers, therefore the *AS* splitting generally derives from the lowest barrier pathway. This barrier is estimated at 157 cm^{-1} on VRT(ASP-W)[18] and 222 cm^{-1} on SAPT-5st[5], while no value is available for MCY-5f.

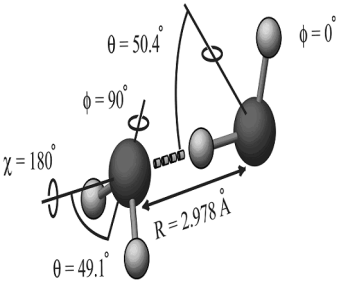

Figure 1. Water dimer molecule – the water dimer is a nonrigid, near-prolate top with two water molecules bound by one quasi-linear hydrogen bond [8]. One monomer acts as a single hydrogen bond acceptor, while the other acts as a single hydrogen bond donor. The nonrigid nature of the water dimer results in its undergoing large amplitude tunneling motions that exchange the protons of the acceptor (*AS*) or of the donor (*BT*) molecule or interchange the roles of the acceptor and the donor molecules themselves (I). All tunneling pathways have been shown to involve motions of both water monomers.

These values are comparable to those found through recent *ab initio* calculations, namely 181 cm^{-1} [19, 20]. It is interesting to note that despite the significant discrepancy in barrier heights, these two potentials agree fairly well on the resulting *AS* splitting for the $K_a = 0$, $J = 0$ level of $(D_2O)_2$ after tuning to related, but different, experimental data, while the *ab initio* values consistently underestimate the experimental value [21].

The *AS* motion effectively splits each $(D_2O)_2$ rovibrational level into two labelled A_1/B_1 or A_2/B_2, while the interchange (*I*) and bifurcation tunneling (*BT*) motions further split/shift these two levels into two sets of three. The six resulting energy levels remain grouped into two sets according to the original *AS* splitting and are henceforth referred to as the 1s and the 2s. For the $K_a = 0$, $J = 0$ level of $(D_2O)_2$, the 1s comprise the states $A_1^+/E_1^+/B_1^+$ whereas the 2s comprise $A_2^-/E_2^-/B_2^-$. It is crucial to note that the numeric label for the doubly degenerate E states is purely one of convenience and does not affect the selection rules as does that of the A and B states: $A_1^+ \leftrightarrow A_1^-$, $A_2^+ \leftrightarrow A_2^-$, $B_1^+ \leftrightarrow B_1^-$, $B_2^+ \leftrightarrow B_2^-$, $E^+ \leftrightarrow E^-$ [9]. It now becomes clear that transitions among *A* and *B* states are only allowed within a given set, while transitions among *E* states transcend this restriction. Nonetheless, the possibility of transitions

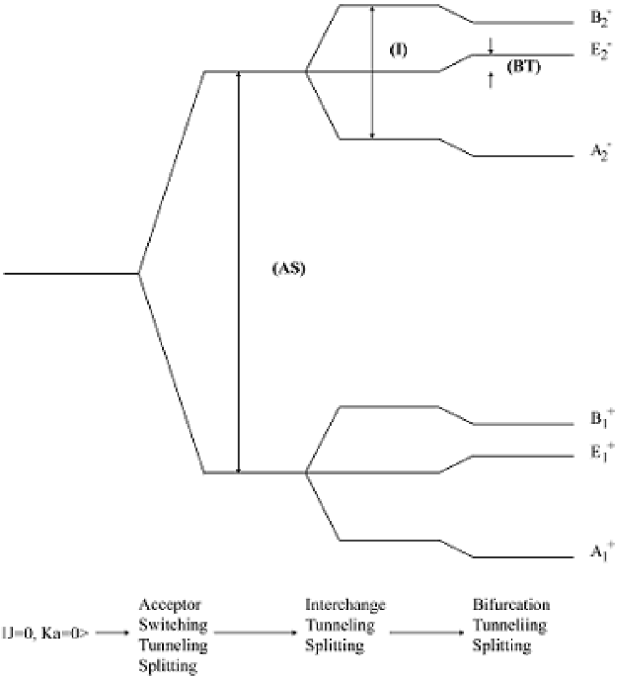

Figure 2. VRT correlation diagram $k'_a = 0$, $j = 0$ – effects of the three tunneling motions on the lowest energy water dimer rovibrational state – not to scale. Bold print indicates tunneling splittings or shifts, regular print indicates symmetry level labelling using the G_{16} permutation-inversion (PI) formalism developed by Dyke [9].

between the 1s and 2s has essentially been ignored and experimental data have been forced to remain divided into two disjoint sets.

In the high barrier limit where E_1^+/E_2^- and E_1^-/E_2^+ states correlate to A' and A' rotational states, $E_2 \leftrightarrow E_1$ transitions are expected to be weak [22]. Indeed since, the permanent dipole moment lies nearly coincident with the plane of symmetry of the water dimer, the pure rotational selection rules are $A' \leftrightarrow A'$ in the vibrational equilibrium C_s structure. However, with decreasing tunneling barriers, coupling of the E_2 and E_1 states becomes large, leading to states that are no longer of a pure A' or A' rotational character, at the same time that contributions of the vibrational component of the dipole moment perpendicular to the plane of symmetry gain importance.

3. Theoretical and experimental considerations

In 1988, Coudert and Hougen determined that matrix elements between A' and A' rovibrational states were not rigorously null in $(H_2O)_2$ [12]. They pointed out that while the high barrier limit was likely to be valid for $(D_2O)_2$, it was not for $(H_2O)_2$ wherein tunneling splittings approach the vibrational frequencies associated with the tunneling motions. They also hypothesized that inclusion of the tunneling motions that accounted for these matrix elements could also engender then unobserved transitions from the upper and lower forks of the 1s, by producing an enhanced interchange splitting of the lower $J=0$, $K_a=0$ levels compared to the upper state levels from which transitions had already been observed. They also suggested that this effect might also account for differences between the interchange splittings of the $K_a=0$ and $K_a=1$ sets of levels. While lower (A_1) and zero (B_1) nuclear spin weights undoubtedly also hindered the early observation of these more weakly allowed transitions, the interchange splittings of the $K_a=0$ and $K_a=1$ ground state levels have since been precisely determined [14, 15, 23] and, for both $(D_2O)_2$ and $(H_2O)_2$, they have been shown to exhibit the types of inequalities that were initially suggested by Coudert and Hougen.

More recently, Smit *et al.* [24] and Leforestier [25] have calculated the actual transition dipole moments for selected E-state transitions (table 1) from the Sapt-5st and MCY-5f potential energy surfaces, respectively. Calculated frequencies agree well each other and with experiment. Of particular note, however, are the strengths of transitions between E_2 and E_1 states. While the dipole moments for these transitions are calculated to be from one to three orders of magnitude weaker than those that remain within a given AS fork, they are by no means negligible.

Given that the line strength is proportional to the square of the transition dipole moment, one would expect line strengths two to six orders of magnitude smaller than that of the weakest, previously measured ground state transition, $E_2^-\ (0,0) \rightarrow E_2^+\ (1,1)$. This particular E_2 transition was observed by both Karyakin *et al.* [26] using an EROS (electric resonance optothermal spectroscopy) technique and by Keutsch *et al.* [27] using a single pass, pulsed nozzle, direct microwave absorption technique. While a signal to noise ratio is not available from the former study, the latter recorded the transition at ~50:1 in a N_2 expansion which is less favourable than an Ar expansion for this type of low K'a transition by a factor of about 100 [25]. For comparison, the strongest reported transition by Keutsch *et al.* was the $E_1^-\ (9,0) \rightarrow E_1^+\ (10,0)$ transition at 108501.2 MHz, which in Ar exhibited a signal to noise

Table 1. Ground state $(D_2O)_2$ transition moments, predicted and observed frequencies.

	Smit *et al.**		Leforestier†		Exp.
$E_i\ (J,\ K_a) \rightarrow E_f\ (J,\ K_a)$	μ (10^{-30} C m)	Freq. (cm^{-1})	μ (10^{-30} C m)	Freq. (cm^{-1})	Freq. (cm^{-1})
$E_1^+\ (0,0) \rightarrow E_1^-\ (1,0)$	7.56	0.37	7.57	0.38	0.36‡
$E_1^+\ (0,0) \rightarrow E_1^-\ (1,1)$	1.08	5.48	1.00	5.25	5.54§
$E_2^-\ (0,0) \rightarrow E_2^+\ (1,1)$	0.941	3.23	0.867	3.25	3.15§,‖
$E_1^+\ (0,0) \rightarrow E_2^-\ (1,1)$	0.017	4.93	0.006	5.04	
$E_2^-\ (0,0) \rightarrow E_1^+\ (1,1)$	0.002	3.78	0.003	3.47	
$E_2^+\ (1,1) \rightarrow E_1^-\ (1,1)$	0.187	0.55	0.091	0.21	

*Reference [24].
†Reference [25].
‡Reference [30].
§Reference [26].
‖Reference [27].

ratio of 10000:1 [27]. While experiment shows that transitions from E_2 states are typically about 10% weaker than analogous transitions from E_1 states [27], this expected decrease in the signal to noise should be somewhat mitigated by the Ar-favoured low J value of the E_2 transition. One might thereby expect the weakest calculated transition, $E_2^- (0,0) \rightarrow E_2^+ (1,1)$, to have a signal to noise ratio of ~5000–10000:1 in an Ar expansion and most importantly for ultraweak $E_2 \leftrightarrow E_1$ transitions to be observable with our current experimental setup.

Additionally, we have reason to believe that $E_2 \leftrightarrow E_1$ transitions with comparable calculated transition dipole moments have already been observed using a less sensitive instrument. Keutsch *et al.* [28] recently proposed the assignment of $E_2 \rightarrow E_1$ transitions as a solution to a long standing discrepancy between theory and experiment. Keutsch argued that the E_2-states attributed to the $(H_2O)_2$ in-plane bend (IPB) normal mode by Braly *et al.* [14] in 2001 were more probably attributable to $E_2 \rightarrow E_1$ transitions from the $K'_a = 0,1$ ground states to the $K'_a = 0$ donor-torsion (DT) vibrationally excited state. Leforestier *et al.* [25] calculated the transition dipole moments for the observed transitions originating in $J = 0$ and 1 states; the values ranged from 0.195×10^{-30} to 0.485×10^{-30} C m. In addition, $(D_2O)_2$ transitions with smaller calculated transition dipole moments will necessarily be more readily observable since the nuclear spin weights of $(D_2O)_2$ E-states are six times greater than those of $(H_2O)_2$. While this assignment has not yet been confirmed, we also recently used the same FIR setup to observe and assign $(H_2O)_2$ hydrogen-bond stretch (S) transitions that have calculated transition dipole moments similar in magnitude to those of the proposed $E_2 \rightarrow E_1$ DT transitions.

Lastly, technological advances continue to push the threshold of sensitivity. A new type of spectrometer powered by an OROTRON was recently developed [29] at Cologne for the probing of van der Waals complexes such as the water dimer. This new millimetre-wave, intracavity-jet OROTRON-spectrometer boasts a sensitivity enhanced by at least one order of magnitude above that of our FIR setup, and at least two orders of magnitude above that of single-pass microwave spectrometer designs such as ours, covers frequencies from 90–330 GHz, and is expected to reach THz frequencies in the near future. Hence, it seems that $E_2 \leftrightarrow E_1$ transitions should be accessible and observable with current OROTRON technologies.

Typically, spectroscopists rely on prominent spectral features such as compact Q-branches for initial spectral assignments, since these tend to be stronger than P and R branches, less prone to power fluctuations, and more complete and easier to identify among other unassigned transitions due to their relatively small spacings. These are especially useful when dealing with weak transitions. The selection rules for E-state dimer transitions are as follows – transitions must obey $+ \leftrightarrow -$ a-type transitions, $\Delta K_a = 0$, are allowed for $\Delta J = \pm 1$, $\Delta K_c = 0$ and for $\Delta J = 0$, ± 1, $\Delta K_c \neq 0$; c-type transitions, $\Delta K_a = 1$ are allowed for $\Delta J = 0, \pm 1$. Thus, one expects a distinct Q-branch for each of the four allowed bands within the $\Delta K_a = 0,1$ stacks: $E_2^{-/+}(K_a = 0) \leftrightarrow E_1^{+/-}(K_a = 1)$, $E_1^{+/-}(K_a = 0) \leftrightarrow E_2^{-/+}(K_a = 1)$, $E_2^{+/-}(K_a = 1) \leftrightarrow E_1^{-/+}(K_a = 1)$, $E_2^{-/+}(K_a = 1) \leftrightarrow E_1^{+/-}(K_a = 1)$. In addition, since transitions between the 1s and the 2s are not allowed for the A and B-states, these bands should be set apart from all others instead of appearing as part of a group of three. A fairly complete picture of the water dimer ground state VRT levels has emerged since the first microwave transitions were reported by Dyke and Muenter in 1974 [8]. With a detailed understanding of the rotational constants, tunneling splittings, and distortion constants that characterize the water dimer energy levels has emerged the possibility of very accurately predicting the spectral 'fingerprint' that will be generated by the ultraweak $E_2 \leftrightarrow E_1$ transitions. Such a fingerprint provides the means for locating and assigning these transitions via matching this precisely predicted fingerprint to experimentally observed transitions, since the absolute frequency of the transitions cannot be predicted with sufficient accuracy.

4. Results

We have compiled all of the published dimer ground state transitions [10, 13, 16, 22, 23, 26, 27, 30–39] along with some recent results reported here for the first time, that pertain to transitions within and among the $K'_a = 0$, 1 and 2 stacks (where K_a is the projection of the rotational quantum number J along the figure axis), and included them in a comprehensive global analysis. A total of 391 and 343 $(D_2O)_2$ and $(H_2O)_2$ lines, respectively, were included in these fits (tables 2a and 2b of Appendix A). Of course the $(D_2O)_2$ and $(H_2O)_2$ data had to be analysed separately since tunneling splittings vary substantially upon isotopic substitution. The 1s and 2s of a given species were included in the same global fit even though the two moieties remain independent without the inclusion of $E_2 \leftrightarrow E_1$ transitions.

The observed transitions were fit to the following near prolate top energy expressions:

$$K_a = 0$$

$$E\left(\frac{A^{\pm}}{B^{\pm}}\right) = \nu^{(0)} \pm \frac{1}{2}I^{(0)} - \frac{1}{2}\nu_{BT}^{(0,1)} + B^{(0)}J(J+1) - D^{(0)}(J(J+1))^2$$

$$E(E^{\pm}) = \nu^{(0)} + \frac{1}{2}\nu_{BT}^{(0,1)} + B^{(0)}J(J+1) - D^{(0)}(J(J+1))^2$$

$$K_a = 1$$

$$E\left(\frac{A^{\pm}}{B^{\pm}}\right) = \nu^{(0,1)} \pm \frac{1}{2}I^{(0)} + \frac{1}{2}\nu_{BT}^{(0,1)} + B^{(1)}(J(J+1)-1) - D^{(1)} \times (J(J+1)-1)^2 \pm \left[\frac{(B-C)^{(1)}}{4} + d^{(1)}J(J+1)\right]J(J+1)$$

$$E(E^{\pm}) = \nu^{(0,1)} - \frac{1}{2}\nu_{BT}^{(0,1)} + B^{(1)}(J(J+1)-1) - D^{(1)}(J(J+1)-1)^2 \pm \left[\frac{(B-C)^{(1)}}{4} + d^{(1)}J(J+1)\right]J(J+1)$$

$$K_a = 2$$

$$E\left(\frac{A^{\pm}}{B^{\pm}}\right) = \nu^{(0,2)} \pm \frac{1}{2}I^{(2)} - \nu_{BT}^{(1,2)} + \frac{1}{2}\nu_{BT}^{(0,1)} + B^{(2)}(J(J+1)-4) - D^{(2)}(J(J+1)-4)^2 \pm \left[\frac{(B-C)^{(2)}}{4}\right]J(J+1)(J-1)(J+2)$$

$$E(E^{\pm}) = \nu^{(0,2)} + \nu_{BT}^{(1,2)} - \frac{1}{2}\nu_{BT}^{(1,2)} + B^{(2)}(J(J+1)-4) - D^{(2)} \times (J(J+1)-4)^2 \pm \left[\frac{(B-C)^{(2)}}{4}\right]J(J+1) \times (J-1)(J+2).$$

*An additional distortion constant, $d^{(1)}$, was required for the $K_a = 1$ levels of $(H_2O)_2$; it is set equal to zero in the case of $(D_2O)_2$. Also for $(H_2O)_2$, the $K_a = 0$ levels and the upper asymmetry components of the $K_a = 1$ levels of the 2s are very close in energy resulting in a Coriolis perturbation between levels of identical symmetry.

The final energy level expression for these states is given by:

$$E(E^{\pm}) = \frac{1}{2}[E^{(0)} + E^{(1)}] \pm \left[\frac{1}{4}(E^{(1)} + E^{(0)})^2 + \zeta^2\left[\frac{1}{2}J(J+1)\right]\frac{1}{2}\right]$$

where $E^{(n)}$ is the unperturbed energy as given above and ζ the Coriolis interaction constant.

$$A^{(0)} = \frac{AS^{(0,1)}}{2} + \nu_{2s}^{(0,1)}$$

$$A^{(2)} = \frac{[\nu_{2s}^{(0,2)} + \nu_{1s}^{(0,2)} - \nu_{2s}^{(0,1)} - \nu_{1s}^{(0,1)}]}{6} + \frac{[\nu_{BT,1s}^{(1,2)} + \nu_{BT,2s}^{(1,2)}]}{6}.$$

Restricted to sums and differences available from c-type transitions: $AS^{(K_a)}$, $\nu^{(K_a)}$, $\nu_{BT}^{(K)}$:

$$\nu_{BT}^{(K_a)}:$$

$$\nu_{1s/2s}^{(0,K_a)} = \left[\nu^{(0)}\frac{1s}{2s} = 0\right] + \nu_{1s/2s}^{(K_a)}. \quad \nu_{BT}^{(K_a-1,K_a)} + \nu_{BT}^{(K_a)}.$$

$$\mathrm{AS}^{(0,1)} = \mathrm{AS}^{(0)} + \mathrm{AS}^{(1)} = \nu_{1s}^{(0,1)} - \nu_{2s}^{(0,1)}.$$

$$\mathrm{AS}^{(1,2)} = \mathrm{AS}^{(2)} - \mathrm{AS}^{(1)} = \nu_{1s}^{(0,2)} - \nu_{2s}^{(0,1)} - \nu_{1s}^{(0,1)} - \nu_{2s}^{(0,1)}.$$

The resulting updated ground state parameters for both $(D_2O)_2$ and $(H_2O)_2$ are presented in table 3a and 3b. It should be noted that since the various K_a stacks are linked via c-type, $\Delta K_a = 1$, transitions, if any one AS splitting is determined, the others may be calculated from the first (figure 3). Although the $K_a = 2$ stack of the 1s of $(H_2O)_2$ is not yet linked by any assigned c-type transitions, which precludes the determination of $AS^{(2)}$, 26 a-type transitions were included in the fit for future reference. With this highly accurate fit and a reasonable estimate of the AS splitting, it is possible to exactly predict the fingerprint of the $E_2 \leftrightarrow E_1$ transitions and to roughly predict its absolute frequency.

As noted above, only the sums and differences, of the AS splittings can be determined from the previously available water dimer ground state data, and then only from c-type transitions. However, Paul *et al.* [7] were able to estimate the individual $K_a = 0$ acceptor switching splitting ($AS^{(0)}$) of the $(D_2O)_2$ ground state through careful analysis of infrared cavity ringdown laser absorption spectra (IR-CRLAS) of the $(D_2O)_2$ hydrogen-bond-acceptor antisymmetric stretch. Paul *et al.* fit the ground and excited state tunneling splitting patterns to a Mathieu equation and determined the $K_a' = 0$ acceptor switching splitting to be ~53 GHz. In an analogous manner, Keutsch [23] estimated the $K_a' = 0$ acceptor switching splitting in $(H_2O)_2$ at ~280 GHz. It should be emphasized that the CRLAS spectral resolution 1 GHz and underlying assumptions of this type of analysis introduce important sources of error in any resulting estimates of the AS splittings, especially in the case of $(H_2O)_2$. Indeed, it was assumed that the ground and excited state tunneling patterns were identical in the

Table 3a. Rotational constants and tunneling splittings of $(D_2O)_2$ (in MHz).

		A_1^+/B_1^-	E_1^+/E_1^-	B_1^+/A_1^-	A_2^-/B_2^+	E_2^-/E_2^+	B_2^-/A_2^+
$K'_a=0$	$B^{(0)}$	5432.585 (9)	5432.34 (1)	5432.145 (9)	5432.542 (9)	5432.38 (1)	5432.230 (9)
	$D^{(0)}$	0.03646 (8)	0.0364 (1)	0.03639 (8)	0.03551 (7)	0.03558 (8)	0.03547 (7)
	$I^{(0)}$		1172.2 (1)			1083.3 (1)	
$K'_a=1$	$A^{(1)}$			124923.6 (1)			
	$\nu^{(0,1)}$		160696.3 (1)			89150.9 (1)	
	$B^{(1)}$	5433.038 (8)	5432.87 (1)	5432.682 (8)	5430.528 (8)	5430.434 (9)	5430.273 (9)
	$D^{(1)}$	0.03575 (6)	0.03564 (8)	0.03566 (7)	0.03535 (6)	0.03550 (7)	0.03536 (6)
	$(B-C)^{(1)}/4$	8.278 (2)	8.280 (2)	8.257 (2)	14.911 (2)	14.884 (2)	14.821 (2)
	$I^{(1)}$		1076.2 (1)			992.3 (1)	
	$\nu^{(0,1)}{}_{BT}$		14.0 (1)			14.15 (9)	
	$AS^{(0,1)}$			71545.4 (1)			
		B_1^-/A_1^+	E_1^-/E_1^+	A_1^-/B_1^+	B_2^+/A_2^-	E_2^+/E_2^-	A_2^+/B_2^-
$K'_a=2$	$A^{(2)}$			125756.7 (8)			
	$\nu^{(0,2)}$		548295.2 (1)			456066.1 (3)	
	$B^{(2)}$	5425.309 (9)	5425.22 (1)	5425.206 (8)	5427.88 (1)	5427.80 (1)	5427.72 (1)
	$D^{(2)}$	0.03455 (7)	0.03445 (7)	0.03449 (6)	0.03543 (8)	0.03539 (7)	0.03517 (8)
	$(B-C)^{(2)}/4$	0.00020 (2)	0.00023 (5)	0.00213 (2)	0.00085 (2)	0.000864 (6)	0.00084 (2)
	$I^{(2)}$		808.6 (2)			801.9 (3)	
	$\nu^{(1,2)}{}_{BT}$		12.85 (7)			13.5 (3)	
	$AS^{(1,2)}$			20683.7(3)			

1σ uncertainty of last significant digit in parenthesis. RMS: 0.283 MHz.

Table 3b. Rotational constants and tunneling splittings of $(H_2O)_2$ (in MHz).

		A_1^+/B_1^-	E_1^+/E_1^-	B_1^+/A_1^-	A_2^-/B_2^+	E_2^-/E_2^+	B_2^-/A_2^+
$K'_a=0$	$B^{(0)}$	6163.92 (4)	6160.60 (3)	6158.31 (5)	6167.6 (4)	6168.23 (5)	6165.97 (3)
	$D^{(0)}$	0.0504 (4)	0.0500 (3)	0.0494 (7)	0.0382 (3)	0.0360 (5)	0.0374 (4)
	$I^{(0)}$		22555.0 (4)			19531.0 (3)	
$K'_a=1$	$A^{(1)}$			227575.1 (4)			
	$\nu^{(0,1)}$		436345.5 (2)			18804.6 (4)	
	$B^{(1)}$	6167.18 (3)	6165.16 (2)	6162.21 (4)	6153.50 (2)	6151.50 (3)	6150.50 (2)
	$D^{(1)}$	0.0499 (3)	0.0495 (2)	0.0489 (5)	0.0538 (2)	0.0544 (2)	0.0543 (3)
	$(B-C)^{(1)}/4$	−1.782 (5)	−1.256 (4)	−1.622 (5)	15.817 (6)	14.12 (1)	13.827 (8)
	$I^{(1)}$		21145.7 (6)			16203.9 (2)	
	$\nu^{(0,1)}{}_{BT}$		1358.6 (2)			1493.5 (4)	
	$AS^{(0,1)}$			417540.9(4)			
	$d^{(1)}$	0*	0*	0*	−0.0062 (10)	−0.0071 (2)	−0.0059 (2)
	ζ	0*	0*	0*	1592.3695[a]	1520.2727[a]	1548.4783[a]
		B_1^-/A_1^+	E_1^-/E_1^+	A_1^-/B_1^+	B_2^+/A_2^-	E_2^+/E_2^-	A_2^+/B_2^-
$K'_a=2$	$A^{(2)}$			N/A			
	$\nu^{(0,2)}$		0*			696321.0 (34)	
	$B^{(2)}$	6145.08 (9)	6144.39 (4)	6142.7 (2)	6156.34 (2)	6155.29 (3)	6154.90 (2)
	$D^{(2)}$	0.0440 (8)	0.0464 (4)	0.039 (2)	0.0501 (2)	0.0502 (2)	0.0495 (2)
	$(B-C)^{(2)}/4$	0.0001 (2)	0.00079 (5)	−0.0000 (2)	0.00108 (4)	0.00110 (1)	0.00084 (6)
	$I^{(2)}$		12225 (3)			11081.4 (3)	
	$\nu^{(1,2)}{}_{BT}$		0*			1383.6 (2)	
	$AS^{(1,2)}$			N/A			

1σ uncertainty of last significant digit in parenthesis. RMS: 0.621 MHz. *Fixed.

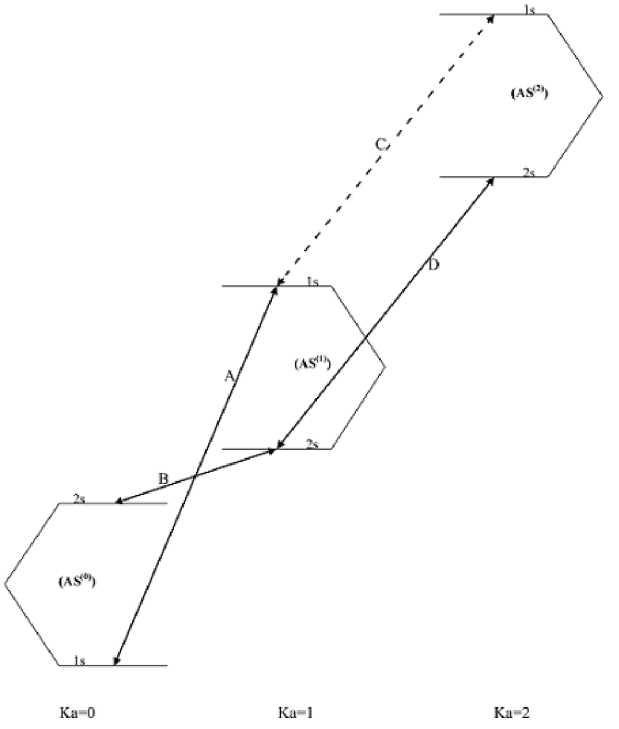

Figure 3. Known C-type transitions linking the K_a stacks of the dimer ground state – known C-type transitions linking the band origins of the 1s and 2s of different K_a stacks; dashed line only known for $(D_2O)_2$. A–$B = AS^{(0)} + AS^{(1)}$; C–D $= AS^{(2)} - AS^{(1)}$.

case of the hydrogen-bond-acceptor antisymmetric stretch, whereas more recent work has shown increases from the ground, $K_a' = 0$, to excited, $K_a^{`} = 0$, state AS splitting of greater than 400 GHz for the more strongly coupled acceptor wag (AW) motion. Hence, this coupling could result in a significant inaccuracy in the AS splittings determined via this approach. The estimated values of 53000 MHz and 279650 MHz for $AS^{(0)}$ of $(D_2O)_2$ and $(H_2O)_2$, respectively, were used in conjunction with the highly accurate rotational constants and tunneling splittings of table 3a and 3b to calculate the fingerprint of the $E_2 \leftrightarrow E_1$ transitions. We provide the relative frequencies for $(H_2O)_2$ and $(D_2O)_2$ in table 4, Appendix B.

5. Discussion

The relative strengths of the four Q-branches may be further modified once E-state specific collisional relaxations are taken into account. Indeed, the E-states are unique in that thermal relaxation is allowed within a K_a stack as well as between stacks [38], such that the $K_a = 1$ E-states may relax to the $K_a = 0$ E-states, leaving the former much less populated than might be expected from simple Boltzmann calculations. The same argument implies that the E_1 ($K_a = 0$) states should be more populated than the E_2 ($K_a = 0$) states and indeed this has been shown experimentally [27]. However, line strength predictions indicate [25] that the E_1 ($K_a = 0$) $\rightarrow E_2$ ($K_a = 1$) P-branch transitions will be weaker than the assigned E_2 ($K_a = 0$) $\rightarrow E_1$ ($K_a = 1$) Q-branch transitions.

6. Summary

We have described here a scenario by which the $(D_2O)_2$ and $(H_2O)_2$ ground state AS tunneling splittings can be determined. We note that the OROTRON spectrometer is uniquely suited to this task. This direct determination of the ground state AS splittings will directly facilitate the refinement of water dimer potential energy surfaces, and will also allow determination of the excited state AS splittings for many of the vibrations already observed, as the spectral data sets are completed. This will facilitate the search for missing excited state subbands that are also important in the quest for a complete and rigorous potential energy surface for the dimer. It is our hope that the E-state transition fingerprints presented in this article will motivate concerted investigations of the ground state of the water dimer and that the critical H_2O dimer acceptor switching splittings will be quantified.

Acknowledgements

This work was supported by the Experimental Physical Chemistry Division of the National Science Foundation.

Appendix A

Table 2a. Fitted $(D_2O)_2$ ground state transitions and residuals (MHz).

J'	K_a'	Γ'	J'	K_a'	Γ′	Frequency	Residual
1	0	A_2^+	0	0	A_2^-	11947.56	−0.06
2	0	B_2^-	1	0	B_2^+	22810.36	−0.1
3	0	A_2^+	2	0	A_2^-	33670.81	−0.18
4	0	B_2^-	3	0	B_2^+	44528.18	−0.15
5	0	A_2^+	4	0	A_2^-	55381.78	0.12
6	0	B_2^-	5	0	B_2^+	66230.49	0.38
7	0	A_2^+	6	0	A_2^-	77072.4	−0.46
8	0	B_2^-	7	0	B_2^+	87909.05	0.01
9	0	A_2^+	8	0	A_2^-	98738	0.18
10	0	B_2^-	9	0	B_2^+	109558.69	0.33
1	0	E_2^+	0	0	E_2^-	10864.49	−0.12
2	0	E_2^-	1	0	E_2^+	21728.17	−0.19
3	0	E_2^+	2	0	E_2^-	32590.14	−0.27
4	0	E_2^-	3	0	E_2^+	43449.5	−0.39
5	0	E_2^+	4	0	E_2^-	54305.83	−0.13
6	0	E_2^-	5	0	E_2^+	65157.9	0.14
7	0	E_2^+	6	0	E_2^-	76004.6	0.17
8	0	E_2^-	7	0	E_2^+	86845.4	0.27
9	0	E_2^+	8	0	E_2^-	97679.3	0.31
10	0	E_2^-	9	0	E_2^+	108505.2	0.03
1	0	B_2^+	0	0	B_2^-	9781.61	−0.03
2	0	A_2^-	1	0	A_2^+	20646.29	−0.06
3	0	B_2^+	2	0	B_2^-	31509.87	−0.11
4	0	A_2^-	3	0	A_2^+	42371.73	0.06
6	0	A_2^-	5	0	A_2^+	64085.7	−0.12
7	0	B_2^+	6	0	B_2^-	74936.5	−0.06
8	0	A_2^-	7	0	A_2^+	85782.1	0.17
9	0	B_2^+	8	0	B_2^-	96621.35	0.27
10	0	A_2^-	9	0	A_2^+	107453.67	0.53
2	1	A_2^+	1	1	A_2^-	22653.02	−0.2
3	1	B_2^-	2	1	B_2^+	33480.67	−0.24
4	1	A_2^+	3	1	A_2^-	44305.51	−0.22
5	1	B_2^-	4	1	B_2^+	55126.96	0.14
6	1	A_2^+	5	1	A_2^-	65943.69	0.35
7	1	B_2^-	6	1	B_2^+	76754.2	−0.23
8	1	A_2^+	7	1	A_2^-	87559.45	0.21
9	1	B_2^-	8	1	B_2^+	98357.35	0.42
10	1	A_2^+	9	1	A_2^-	109147.43	0.8
2	1	B_2^-	1	1	B_2^+	22771.48	0.06
3	1	A_2^+	2	1	A_2^-	33657.78	0.1
4	1	B_2^-	3	1	B_2^+	44540.83	0.14
5	1	A_2^+	4	1	A_2^-	55420	0.38
6	1	B_2^-	5	1	B_2^+	66293.9	0.29
7	1	A_2^+	6	1	A_2^-	77161.8	−0.01
8	1	B_2^-	7	1	B_2^+	88023	−0.38
9	1	A_2^+	8	1	A_2^-	98876.8	−0.65
10	1	B_2^-	9	1	B_2^+	109722.53	−0.65
5	1	E_2^-	4	1	E_2^+	54138.81	0.35
6	1	E_2^+	5	1	E_2^-	64956.67	−0.11
7	1	E_2^-	6	1	E_2^+	75770.1	0.11
8	1	E_2^+	7	1	E_2^-	86577.65	0.42
9	1	E_2^-	8	1	E_2^+	97378.3	0.64
10	1	E_2^+	9	1	E_2^-	108171.52	1.1
2	1	E_2^-	1	1	E_2^+	21780.5	0.08
3	1	E_2^+	2	1	E_2^-	32668.66	0.16
4	1	E_2^-	3	1	E_2^+	43554.09	0.07
5	1	E_2^+	4	1	E_2^-	54436.56	0.42
6	1	E_2^-	5	1	E_2^+	65313.77	−0.22
7	1	E_2^+	6	1	E_2^-	76186.32	−0.41
8	1	E_2^-	7	1	E_2^+	87053.2	−0.31
9	1	E_2^+	8	1	E_2^-	97912.95	−0.52
10	1	E_2^-	9	1	E_2^+	108764.84	−0.92
3	1	A_2^-	2	1	A_2^+	31498.68	−0.04
4	1	B_2^+	3	1	B_2^-	42325.78	−0.07
6	1	B_2^+	5	1	B_2^-	63970.3	0.2
7	1	A_2^-	6	1	A_2^+	74785.7	0.19
8	1	B_2^+	7	1	B_2^-	85595.4	0.07
9	1	A_2^-	8	1	A_2^+	96398.95	0.26
10	1	B_2^+	9	1	B_2^-	107195.15	0.38
11	1	A_2^-	10	1	A_2^+	117983.19	0.49
3	1	B_2^+	2	1	B_2^-	31679.17	0.44
4	1	A_2^-	3	1	A_2^+	42566.73	0.13
6	1	A_2^-	5	1	A_2^+	64333	−0.39
7	1	B_2^+	6	1	B_2^-	75210.9	0.28
8	1	A_2^-	7	1	A_2^+	86082.7	0.09
9	1	B_2^+	8	1	B_2^-	96948.15	−0.37
10	1	A_2^-	9	1	A_2^+	107806.52	−0.97
10	2	A_2^+	9	1	A_2^-	461037.04	0.07
10	2	B_2^-	9	1	B_2^+	458372.22	−0.61
12	2	B_2^-	11	1	B_2^+	479259.12	0.34
10	2	E_2^+	9	1	E_2^-	460178.67	−0.76
10	2	E_2^-	9	1	E_2^+	457520.79	−0.09
11	2	E_2^+	10	1	E_2^-	467989.8	0.77
10	2	B_2^+	9	1	B_2^-	459272.1	0.19
10	2	A_2^-	9	1	A_2^+	456623.95	−0.39
11	2	B_2^+	10	1	B_2^-	467098.41	0.39
4	1	B_2^-	5	0	B_2^+	30718.5	1.11
3	1	B_2^+	4	0	B_2^-	41473.39	0.6
1	1	B_2^-	1	0	B_2^+	84738.25	−0.25
2	1	A_2^+	2	0	A_2^-	84670.15	−0.28
3	1	B_2^-	3	0	B_2^+	84568.05	−0.28
4	1	A_2^+	4	0	A_2^-	84431.9	−0.32
5	1	B_2^-	5	0	B_2^+	84261.85	−0.26
6	1	A_2^+	6	0	A_2^-	84057.7	−0.32
7	1	B_2^-	7	0	B_2^+	83819.88	−0.09
8	1	A_2^+	8	0	A_2^-	83547.81	−0.17
9	1	B_2^-	9	0	B_2^+	83242.12	0.02
10	1	A_2^+	10	0	A_2^-	82902.44	0.09
11	1	B_2^-	11	0	B_2^+	82529.07	0.31
1	1	A_2^+	0	0	A_2^-	95662.7	−0.02
2	1	B_2^-	1	0	B_2^+	106577.4	0.09
3	1	A_2^+	2	0	A_2^-	117515.78	0.34
4	1	E_2^-	5	0	E_2^+	29661.32	0.72
3	1	E_2^+	4	0	E_2^-	40413.02	0.48
1	1	E_2^-	1	0	E_2^+	83672.55	−0.2
2	1	E_2^+	2	0	E_2^-	83605.54	−0.19
3	1	E_2^-	3	0	E_2^+	83505.01	−0.21

(*continued*)

Table 2a. Continued.

J'	K_a'	Γ'	J'	K_a'	Γ′	Frequency	Residual
4	1	E_2^+	4	0	E_2^-	83371	−0.21
5	1	E_2^-	5	0	E_2^+	83203.42	−0.29
6	1	E_2^+	6	0	E_2^-	83002.43	−0.3
7	1	E_2^-	7	0	E_2^+	82768.07	−0.21
8	1	E_2^+	8	0	E_2^-	82500.27	−0.11
9	1	E_2^-	9	0	E_2^+	82198.8	−0.25
10	1	E_2^+	10	0	E_2^-	81864.72	0.42
1	1	E_2^+	0	0	E_2^-	94596.9	0.01
2	1	E_2^-	1	0	E_2^+	105512.72	0.02
3	1	E_2^+	2	0	E_2^-	116453.15	0.31
1	1	A_2^-	1	0	A_2^+	82663.35	−0.21
2	1	B_2^+	2	0	B_2^-	82597.16	−0.24
3	1	A_2^-	3	0	A_2^+	82497.98	−0.18
4	1	B_2^+	4	0	B_2^-	82365.72	−0.13
5	1	A_2^-	5	0	A_2^+	82200.38	−0.11
6	1	B_2^+	6	0	B_2^-	82001.84	−0.25
7	1	A_2^-	7	0	A_2^+	81770.54	−0.13
8	1	B_2^+	8	0	B_2^-	81506.25	0
9	1	A_2^-	9	0	A_2^+	81208.68	−0.18
10	1	B_2^+	10	0	B_2^-	80878.62	0.11
1	1	B_2^+	0	0	B_2^-	93587.6	0.08
3	1	B_2^+	2	0	B_2^-	115446.25	0.68
5	2	B_2^-	4	2	B_2^+	55061.63	0.3
6	2	A_2^+	5	2	A_2^-	65903.99	1.3
7	2	B_2^-	6	2	B_2^+	76738.4	−0.24
8	2	A_2^+	7	2	A_2^-	87568.25	−0.09
9	2	B_2^-	8	2	B_2^+	98390.85	−0.12
10	2	A_2^+	9	2	A_2^-	109205.3	−0.42
5	2	A_2^+	4	2	A_2^-	55061.63	−0.49
6	2	B_2^-	5	2	B_2^+	65903.99	−0.09
7	2	A_2^+	6	2	A_2^-	76740.6	−0.25
8	2	B_2^-	7	2	B_2^+	87571.7	0.06
9	2	A_2^+	8	2	A_2^-	98395.7	0.03
10	2	B_2^-	9	2	B_2^+	109211.87	−0.29
5	2	E_2^-	4	2	E_2^+	54263.41	0.72
6	2	E_2^+	5	2	E_2^-	65106.12	0.47
7	2	E_2^-	6	2	E_2^+	75943.4	0
8	2	E_2^+	7	2	E_2^-	86775.05	−0.01
9	2	E_2^-	8	2	E_2^+	97599.6	−0.15
10	2	E_2^+	9	2	E_2^-	108416.32	−0.29
5	2	E_2^+	4	2	E_2^-	54263.41	−0.11
6	2	E_2^-	5	2	E_2^+	65107.2	0.1
7	2	E_2^+	6	2	E_2^-	75945.62	−0.1
8	2	E_2^-	7	2	E_2^+	86778.5	−0.04
9	2	E_2^+	8	2	E_2^-	97604.5	−0.23
10	2	E_2^-	9	2	E_2^+	108423.11	−0.35
5	2	E_2^+	5	2	E_2^-	1.4	−0.05
6	2	E_2^-	6	2	E_2^+	2.9	0
7	2	E_2^+	7	2	E_2^-	5.2	−0.02
8	2	E_2^-	8	2	E_2^+	8.65	−0.06
9	2	E_2^+	9	2	E_2^-	13.55	−0.13
10	2	E_2^-	10	2	E_2^+	20.3	−0.22
11	2	E_2^+	11	2	E_2^-	29.29	−0.35
6	2	B_2^+	5	2	B_2^-	64309.3	0.39

Table 2a. Continued.

J'	K_a'	Γ'	J'	K_a'	Γ′	Frequency	Residual
7	2	A_2^-	6	2	A_2^+	75148.7	0.11
8	2	B_2^+	7	2	B_2^-	85982.2	−0.17
9	2	A_2^-	8	2	A_2^+	96809	−0.34
10	2	B_2^+	9	2	B_2^-	107628.32	−0.25
6	2	A_2^-	5	2	A_2^+	64310.7	0.34
7	2	B_2^+	6	2	B_2^-	75151	0.09
8	2	A_2^-	7	2	A_2^+	85985.7	−0.16
9	2	B_2^+	8	2	B_2^-	96814.1	−0.24
10	2	A_2^-	9	2	A_2^+	107635.24	−0.23
2	2	E_2^+	2	1	E_2^-	350543.41	−0.2
3	2	E_2^-	3	1	E_2^+	350439.37	−0.32
4	2	E_2^+	4	1	E_2^-	350300.63	−0.41
5	2	E_2^-	5	1	E_2^+	350127	−0.59
6	2	E_2^+	6	1	E_2^-	349918.63	−0.63
2	2	E_2^-	1	1	E_2^+	372324.02	−0.05
3	2	E_2^+	2	1	E_2^-	383108.23	−0.16
4	2	E_2^-	3	1	E_2^+	393855.36	−0.32
5	2	E_2^+	4	1	E_2^-	404564.74	−0.43
6	2	E_2^-	5	1	E_2^+	415235.58	−0.57
2	2	E_2^-	2	1	E_2^+	350722.4	0.14
3	2	E_2^+	3	1	E_2^-	350797.43	0.33
4	2	E_2^-	4	1	E_2^+	350897.51	0.5
5	2	E_2^+	5	1	E_2^-	351022.61	0.55
6	2	E_2^-	6	1	E_2^+	351172.94	0.55
2	2	E_2^+	1	1	E_2^-	372383.62	0.06
3	2	E_2^-	2	1	E_2^+	383286.97	0.18
4	2	E_2^+	3	1	E_2^-	394212.61	0.34
5	2	E_2^-	4	1	E_2^+	405159.59	0.52
6	2	E_2^+	5	1	E_2^-	416126.84	0.57
1	0	A_1^-	0	0	A_1^+	12036.27	−0.03
2	0	B_1^+	1	0	B_1^-	22898.62	−0.08
3	0	A_1^-	2	0	A_1^+	33758.33	−0.13
4	0	B_1^+	3	0	B_1^-	44614.57	−0.17
5	0	A_1^-	4	0	A_1^+	55466.89	0.24
6	0	B_1^+	5	0	B_1^-	66313.53	0.2
7	0	A_1^-	6	0	A_1^+	77154	0.08
8	0	B_1^+	7	0	B_1^-	87987.4	−0.16
9	0	A_1^-	8	0	A_1^+	98813.35	−0.02
10	0	B_1^+	9	0	B_1^-	109630.55	0.04
1	0	E_1^-	0	0	E_1^+	10864.49	−0.05
2	0	E_1^+	1	0	E_1^-	21728.17	−0.03
3	0	E_1^-	2	0	E_1^+	32590.14	0.02
4	0	E_1^+	3	0	E_1^-	43449.5	0.08
5	0	E_1^-	4	0	E_1^+	54305.83	0.61
6	0	E_1^+	5	0	E_1^-	65156.7	0.05
7	0	E_1^-	6	0	E_1^+	76002.8	−0.03
8	0	E_1^+	7	0	E_1^-	86842.92	0.02
9	0	E_1^-	8	0	E_1^+	97675.9	−0.08
10	0	E_1^+	9	0	E_1^-	108501.2	0.01
1	0	B_1^-	0	0	B_1^+	9692.87	0
2	0	A_1^+	1	0	A_1^-	20557.88	−0.02
3	0	B_1^-	2	0	B_1^+	31422	−0.05
4	0	A_1^+	3	0	A_1^-	42284.43	−0.03
6	0	A_1^+	5	0	A_1^-	64000.6	0.11

(*continued*)

Table 2a. Continued.

J'	$K_a^{`}$	Γ'	J''	K_a''	Γ''	Frequency	Residual
7	0	B_1^-	6	0	B_1^+	74852.4	0.05
8	0	A_1^+	7	0	A_1^-	85699.2	0.26
9	0	B_1^-	8	0	B_1^+	96539.3	−0.05
10	0	A_1^+	9	0	A_1^-	107372.62	−0.08
2	1	A_1^-	1	1	A_1^+	22772.72	−0.03
3	1	B_1^+	2	1	B_1^-	33617.61	−0.08
4	1	A_1^-	3	1	A_1^+	44459.31	−0.1
5	1	B_1^+	4	1	B_1^-	55297.32	0.28
6	1	A_1^-	5	1	A_1^+	66130.16	0.41
7	1	B_1^+	6	1	B_1^-	76956.7	0.02
8	1	A_1^-	7	1	A_1^+	87777.05	0.05
9	1	B_1^+	8	1	B_1^-	98590.05	0.19
10	1	A_1^-	9	1	A_1^+	109394.44	0.01
2	1	B_1^+	1	1	B_1^-	22838.68	−0.04
3	1	A_1^-	2	1	A_1^+	33716.43	−0.1
4	1	B_1^+	3	1	B_1^-	44590.92	−0.1
7	1	A_1^-	6	1	A_1^+	77186.1	−0.02
8	1	B_1^+	7	1	B_1^-	88038.8	−0.08
9	1	A_1^-	8	1	A_1^+	98884.05	−0.04
10	1	B_1^+	9	1	B_1^-	109721	0.07
5	1	E_1^+	4	1	E_1^-	54229.01	0.22
6	1	E_1^-	5	1	E_1^+	65064.8	−0.34
7	1	E_1^+	6	1	E_1^-	75896.2	−0.16
8	1	E_1^-	7	1	E_1^+	86721.69	0.1
9	1	E_1^+	8	1	E_1^-	97540.09	0.11
10	1	E_1^-	9	1	E_1^+	108350.7	0.03
2	1	E_1^+	1	1	E_1^-	21763.7	−0.04
3	1	E_1^-	2	1	E_1^+	32643.46	−0.01
5	1	E_1^-	4	1	E_1^+	54394.67	0.28
6	1	E_1^+	5	1	E_1^-	65263.63	−0.22
7	1	E_1^-	6	1	E_1^+	76128	−0.19
8	1	E_1^+	7	1	E_1^-	86986.56	0.02
9	1	E_1^-	8	1	E_1^+	97838.07	0.02
10	1	E_1^+	9	1	E_1^-	108681.9	0.04
3	1	A_1^+	2	1	A_1^-	31470.41	−0.16
4	1	B_1^-	3	1	B_1^+	42316.8	−0.14
6	1	B_1^-	5	1	B_1^+	64000.6	0.11
7	1	A_1^+	6	1	A_1^-	74835.8	−0.14
8	1	B_1^-	7	1	B_1^+	85665.95	−0.05
9	1	A_1^+	8	1	A_1^-	96489.9	0.08
10	1	B_1^-	9	1	B_1^+	107306.61	0.11
3	1	B_1^-	2	1	B_1^+	31570.01	−0.14
4	1	A_1^+	3	1	A_1^-	42449.73	−0.16
6	1	A_1^+	5	1	A_1^-	64200.71	0.28
7	1	B_1^-	6	1	B_1^+	75069.4	−0.09
8	1	A_1^+	7	1	A_1^-	85933.15	−0.1
9	1	B_1^-	8	1	B_1^+	96790.75	−0.1
10	1	A_1^+	9	1	A_1^-	107641.51	0.11
6	1	B_1^+	7	0	B_1^-	80750.91	−0.01
5	1	A_1^-	6	0	A_1^+	91495.8	0.04
4	1	B_1^+	5	0	B_1^-	102263.05	0.04
3	1	A_1^-	4	0	A_1^+	113051.75	0.08
1	1	B_1^+	1	0	B_1^-	156385.64	0.03
2	1	A_1^-	2	0	A_1^+	156353.37	0.08

Table 2a. Continued.

J'	$K_a^{`}$	Γ'	J''	K_a''	Γ''	Frequency	Residual
3	1	B_1^+	3	0	B_1^-	156304.88	0.04
4	1	A_1^-	4	0	A_1^+	156240.39	0.05
5	1	B_1^+	5	0	B_1^-	156159.89	0.03
1	1	A_1^-	0	0	A_1^+	167283.51	−0.16
6	1	E_1^+	7	0	E_1^-	79620.9	0.04
5	1	E_1^-	6	0	E_1^+	90359.82	−0.02
4	1	E_1^+	5	0	E_1^-	101122.13	0.03
3	1	E_1^-	4	0	E_1^+	111906.7	0.02
2	1	E_1^-	2	0	E_1^+	155203.41	0.02
3	1	E_1^+	3	0	E_1^-	155157.42	0.04
4	1	E_1^-	4	0	E_1^+	155096.24	0.11
1	1	E_1^-	0	0	E_1^+	166131.5	−0.25
6	1	A_1^+	7	0	A_1^-	78542.3	0.03
5	1	B_1^-	6	0	B_1^+	89276.73	0.12
4	1	A_1^+	5	0	A_1^-	100035.05	0.14
3	1	B_1^-	4	0	B_1^+	110815.4	−0.82
1	1	A_1^+	1	0	A_1^-	154138.53	0.09
2	1	B_1^-	2	0	B_1^+	154109.28	0.08
3	1	A_1^+	3	0	A_1^-	154065.46	0.07
4	1	B_1^-	4	0	B_1^+	154007.11	0.06
5	2	B_1^+	4	2	B_1^-	55044.77	0.34
6	2	A_1^-	5	2	A_1^+	65882.15	0.41
7	2	B_1^+	6	2	B_1^-	76714.1	0.23
8	2	A_1^-	7	2	A_1^+	87539.85	−0.13
9	2	B_1^+	8	2	B_1^-	98359.1	−0.15
10	2	A_1^-	9	2	A_1^+	109170.68	−0.17
5	2	A_1^-	4	2	A_1^+	55044.77	0.13
6	2	B_1^+	5	2	B_1^-	65882.15	0.03
7	2	A_1^-	6	2	A_1^+	76714.1	−0.38
8	2	B_1^+	7	2	B_1^-	87540.85	−0.06
9	2	A_1^-	8	2	A_1^+	98360.55	−0.05
10	2	B_1^+	9	2	B_1^-	109172.85	0.13
5	2	E_1^+	4	2	E_1^-	54238.01	0.35
6	2	E_1^-	5	2	E_1^+	65075.9	−0.13
7	2	E_1^+	6	2	E_1^-	75909.7	0.28
8	2	E_1^-	7	2	E_1^+	86737.03	0.06
9	2	E_1^+	8	2	E_1^-	97557.9	0.03
10	2	E_1^-	9	2	E_1^+	108371.17	−0.11
5	2	E_1^-	4	2	E_1^+	54238.01	0.14
6	2	E_1^+	5	2	E_1^-	65075.9	−0.52
7	2	E_1^-	6	2	E_1^+	75909.7	−0.33
8	2	E_1^+	7	2	E_1^-	86737.93	0.04
9	2	E_1^-	8	2	E_1^+	97559.2	0.01
10	2	E_1^+	9	2	E_1^-	108373.1	0.01
5	2	E_1^-	5	2	E_1^+	0.42	0.04
6	2	E_1^+	6	2	E_1^-	0.76	−0.01
7	2	E_1^-	7	2	E_1^+	1.4	0.02
8	2	E_1^+	8	2	E_1^-	2.3	0
9	2	E_1^-	9	2	E_1^+	3.6	−0.02
10	2	E_1^+	10	2	E_1^-	5.43	0
11	2	E_1^-	11	2	E_1^+	7.82	−0.02
12	2	E_1^+	12	2	E_1^-	11.05	0.07
6	2	B_1^-	5	2	B_1^+	64271.4	0.33
7	2	A_1^+	6	2	A_1^-	75105.8	0.01

(*continued*)

Table 2a. Continued.

J'	K_a'	Γ'	J''	K_a''	Γ''	Frequency	Residual
8	2	B_1^-	7	2	B_1^+	85934.63	−0.24
9	2	A_1^+	8	2	A_1^-	96757.23	−0.22
10	2	B_1^-	9	2	B_1^+	107572.5	−0.2
6	2	A_1^+	5	2	A_1^-	64271.4	0.02
7	2	B_1^-	6	2	B_1^+	75105.8	−0.49
8	2	A_1^+	7	2	A_1^-	85935.53	−0.07
9	2	B_1^-	8	2	B_1^+	96758.4	−0.09
10	2	A_1^+	9	2	A_1^-	107574.3	0.2
2	2	A_1^-	2	1	A_1^+	372164.77	0.04
3	2	B_1^+	3	1	B_1^-	372069.49	0.08
4	2	A_1^-	4	1	A_1^+	371942.44	0.01
5	2	B_1^+	5	1	B_1^-	371783.88	−0.02
2	2	B_1^+	1	1	B_1^-	393929.15	0.01
3	2	A_1^-	2	1	A_1^+	404713.88	−0.04
4	2	B_1^+	3	1	B_1^-	415464.45	−0.08
5	2	A_1^-	4	1	A_1^+	426180.13	−0.13
8	2	B_1^+	7	1	B_1^-	458111.37	−0.1
10	2	B_1^+	9	1	B_1^-	479213.04	0.08
2	2	B_1^+	2	1	B_1^-	372264.07	0
3	2	A_1^-	3	1	A_1^+	372268.17	0.04
4	2	B_1^+	4	1	B_1^-	372273.67	−0.03
5	2	A_1^-	5	1	A_1^+	372280.87	−0.07
2	2	A_1^-	1	1	A_1^+	393962.28	0.03
3	2	B_1^+	2	1	B_1^-	404813.17	−0.04
4	2	A_1^-	3	1	A_1^+	415662.69	−0.36
5	2	B_1^+	4	1	B_1^-	426510.84	−0.18
8	2	A_1^-	7	1	A_1^+	459036.11	−0.36
12	2	A_1^-	11	1	A_1^+	502335.92	0.05
2	2	E_1^-	2	1	E_1^+	371248.93	0.04
3	2	E_1^+	3	1	E_1^-	371154.77	0.09
4	2	E_1^-	4	1	E_1^+	371029.15	−0.01
5	2	E_1^+	5	1	E_1^-	370872.5	0.07
2	2	E_1^+	1	1	E_1^-	393012.64	−0.01
3	2	E_1^-	2	1	E_1^+	403798.16	−0.04
4	2	E_1^+	3	1	E_1^-	414549.95	−0.01
5	2	E_1^-	4	1	E_1^+	425267.19	−0.01
8	2	E_1^+	7	1	E_1^-	457205.44	0.32
9	2	E_1^-	8	1	E_1^+	467777.48	−0.28
2	2	E_1^+	2	1	E_1^-	371348.24	−0.02
3	2	E_1^-	3	1	E_1^+	371353.46	0.02
4	2	E_1^+	4	1	E_1^-	371360.51	0
5	2	E_1^-	5	1	E_1^+	371369.52	−0.08
2	2	E_1^-	1	1	E_1^+	393045.73	−0.02
3	2	E_1^+	2	1	E_1^-	403897.49	−0.02
4	2	E_1^-	3	1	E_1^+	414748.48	−0.03
5	2	E_1^+	4	1	E_1^-	425597.94	−0.06
8	2	E_1^-	7	1	E_1^+	458130.13	−0.01
11	2	E_1^+	10	1	E_1^-	490623.48	0.07
2	2	B_1^-	2	1	B_1^+	370282.21	0.18
3	2	A_1^+	3	1	A_1^-	370189.67	0.09
4	2	B_1^-	4	1	B_1^+	370066.38	−0.03
5	2	A_1^+	5	1	A_1^-	369912.5	−0.11
2	2	A_1^+	1	1	A_1^-	392045.05	0.11
3	2	B_1^-	2	1	B_1^+	402831.91	0.07
4	2	A_1^+	3	1	A_1^-	413585.42	−0.09
5	2	B_1^-	4	1	B_1^+	424305.09	−0.14
8	2	A_1^+	7	1	A_1^-	456253.76	−0.08
9	2	B_1^-	8	1	B_1^+	466831.18	0.1
2	2	A_1^+	2	1	A_1^-	370381.32	0.2
3	2	B_1^-	3	1	B_1^+	370387.86	0.07
4	2	A_1^+	4	1	A_1^-	370396.8	−0.04
5	2	B_1^-	5	1	B_1^+	370408.33	−0.04
2	2	B_1^-	1	1	B_1^+	392078.06	0.1
3	2	A_1^+	2	1	A_1^-	402930.86	−0.01
4	2	B_1^-	3	1	B_1^+	413783.45	−0.09
5	2	A_1^+	4	1	A_1^-	424635	−0.17
8	2	B_1^-	7	1	B_1^+	457178.06	1.45
9	2	A_1^+	8	1	A_1^-	468016.4	−0.51

Γ: symmetry species of the level in the molecular symmetry group G_{16}.
RMS: 0.283 MHz
Negative frequencies indicate emissions, as written, since the transition is based on the experimentally determined zero frequency.

Table 2b. Fitted $(H_2O)_2$ ground state transitions and residuals (MHz).

J'	K_a'	Γ'	J''	K_a''	Γ''	Frequency	Residual
1	0	A_2^+	0	0	A_2^-	31673.4	−0.18
2	0	B_2^-	1	0	B_2^+	43797.03	−0.08
3	0	A_2^+	2	0	A_2^-	55916.67	−0.15
4	0	B_2^-	3	0	B_2^+	68043.3	−0.34
5	0	A_2^+	4	0	A_2^-	80182.5	−0.24
6	0	B_2^-	5	0	B_2^+	92334.4	−0.16
7	0	A_2^+	6	0	A_2^-	104496.4	−0.24
8	0	B_2^-	7	0	B_2^+	116665	−0.14
1	0	E_2^+	0	0	E_2^-	12132.81	−0.01
2	0	E_2^-	1	0	E_2^+	24284.32	−0.05
3	0	E_2^+	2	0	E_2^-	36464.94	−0.05
4	0	E_2^-	3	0	E_2^+	48675.12	−0.1
5	0	E_2^+	4	0	E_2^-	60910	0.42
6	0	E_2^-	5	0	E_2^+	73160.8	0.02
7	0	E_2^+	6	0	E_2^-	85422.1	0.11
8	0	E_2^-	7	0	E_2^+	97687.2	−0.33
9	0	E_2^+	8	0	E_2^-	109953	0.12
1	0	B_2^+	0	0	B_2^-	−7354.86	−0.01
2	0	A_2^-	1	0	A_2^+	4863.16	−0.11
3	0	B_2^+	2	0	B_2^-	17122.62	−0.19
4	0	A_2^-	3	0	A_2^+	29416.39	−0.23
5	0	B_2^+	4	0	B_2^-	41734.73	−0.25
6	0	A_2^-	5	0	A_2^+	54068.53	−0.23
7	0	B_2^+	6	0	B_2^-	66410.42	−0.29
8	0	A_2^-	7	0	A_2^+	78755.73	0.21
9	0	B_2^+	8	0	B_2^-	91099.7	0.26

(*continued*)

Table 2b. Continued.

J"	$K_a^{"}$	Γ"	J′	K_a'	Γ′	Frequency	Residual
10	0	A_2^-	9	0	A_2^+	103439.8	0.04
11	0	B_2^+	10	0	B_2^-	115774.4	−0.12
5	1	A_2^+	6	0	A_2^-	−36804.25	0.1
4	1	B_2^-	5	0	B_2^+	−25899.06	0.25
3	1	A_2^+	4	0	A_2^-	−14826.98	0.09
1	1	B_2^-	1	0	B_2^+	32112.47	0.27
2	1	A_2^+	2	0	A_2^-	32297.22	0.11
3	1	B_2^-	3	0	B_2^+	32553.28	−0.03
4	1	A_2^+	4	0	A_2^-	32860.8	−0.18
5	1	B_2^-	5	0	B_2^+	33199.97	−0.18
6	1	A_2^+	6	0	A_2^-	33552.54	−0.1
7	1	B_2^-	7	0	B_2^+	33903.33	0.37
6	1	B_2^-	5	0	B_2^+	111166.97	−0.08
4	0	E_2^-	3	1	E_2^+	35286.6	−0.07
3	0	E_2^+	2	1	E_2^-	24139.64	−0.02
1	0	E_2^+	2	1	E_2^-	−36609.62	0.08
2	1	A_2^-	1	0	A_2^+	21616.23	0.18
3	1	B_2^+	2	0	B_2^-	34768.42	0.09
5	1	B_2^+	4	0	B_2^-	61814.56	−0.07
6	1	A_2^-	5	0	A_2^+	75613.1	−0.08
7	1	B_2^+	6	0	B_2^-	89541.2	−0.46
8	1	A_2^-	7	0	A_2^+	103569	−0.09
9	1	B_2^+	8	0	B_2^-	117670.8	−0.18
1	1	A_2^+	1	1	A_2^-	16449.42	0.06
2	1	B_2^-	2	1	B_2^+	16918.53	0.02
3	1	A_2^+	3	1	A_2^-	17588.41	−0.01
4	1	B_2^-	4	1	B_2^+	18430.4	−0.08
5	1	A_2^+	5	1	A_2^-	19418.12	−0.26
3	1	B_2^-	2	1	B_2^+	53015.86	−0.38
4	1	A_2^+	3	1	A_2^-	65275.95	−0.53
5	1	B_2^-	4	1	B_2^+	77529	−0.94
6	1	A_2^+	5	1	A_2^-	89775	−0.38
7	1	B_2^-	6	1	B_2^+	102011.6	0.06
8	1	A_2^+	7	1	A_2^-	114238	0.84
1	1	B_2^-	1	1	B_2^+	15982.87	0.01
2	1	A_2^+	2	1	A_2^-	15544.2	−0.13
3	1	B_2^-	3	1	B_2^+	14907.53	−0.26
4	1	A_2^+	4	1	A_2^-	14092.8	−0.33
5	1	B_2^-	5	1	B_2^+	13120.21	−0.29
6	1	A_2^+	6	1	A_2^-	12008.18	−0.05
7	1	B_2^-	7	1	B_2^+	10772.51	0.5
3	1	A_2^+	2	1	A_2^-	53753.29	−0.3
4	1	B_2^-	3	1	B_2^+	66233.2	−0.58
5	1	A_2^+	4	1	A_2^-	78678.6	−0.69
6	1	B_2^-	5	1	B_2^+	91086.8	−0.6
7	1	A_2^+	6	1	A_2^-	103458	−0.31
8	1	B_2^-	7	1	B_2^+	115793.6	−0.01
2	1	E_2^+	1	1	E_2^-	24548.3	−0.17
3	1	E_2^-	2	1	E_2^+	36819.84	−0.02
4	1	E_2^+	3	1	E_2^-	49087.38	−0.48
5	1	E_2^-	4	1	E_2^+	61351.8	0.49
6	1	E_2^+	5	1	E_2^-	73609.16	0.06
7	1	E_2^-	6	1	E_2^+	85860.15	0.07
8	1	E_2^+	7	1	E_2^-	98102.8	−0.31

Table 2b. Continued.

J"	$K_a^{"}$	Γ"	J′	K_a'	Γ′	Frequency	Residual
9	1	E_2^-	8	1	E_2^+	110336.84	−0.24
2	1	E_2^-	1	1	E_2^+	25048.44	0.11
3	1	E_2^+	2	1	E_2^-	37528.94	0.74
4	1	E_2^-	3	1	E_2^+	49971.38	−0.08
6	1	E_2^+	5	1	E_2^-	74762.4	−0.07
7	1	E_2^-	6	1	E_2^+	87119.55	−0.12
8	1	E_2^+	7	1	E_2^-	99456	−0.17
9	1	E_2^-	8	1	E_2^+	111774.02	−0.12
1	1	E_2^+	1	1	E_2^-	259.92	0.02
2	1	E_2^-	2	1	E_2^+	759.74	−0.02
3	1	E_2^+	3	1	E_2^-	1468.08	−0.03
4	1	E_2^-	4	1	E_2^+	2351.68	−0.04
5	1	E_2^+	5	1	E_2^-	3381.64	0
2	1	B_2^+	1	1	B_2^-	8344.46	−0.33
3	1	A_2^-	2	1	A_2^+	20620.65	−0.18
4	1	B_2^+	3	1	B_2^-	32895.28	−0.24
5	1	A_2^-	4	1	A_2^+	45167.86	0.08
6	1	B_2^+	5	1	B_2^-	57436.73	0.19
7	1	A_2^-	6	1	A_2^+	69701.5	0.76
8	1	B_2^+	7	1	B_2^-	81959.55	0.19
9	1	A_2^-	8	1	A_2^+	94211.8	0.41
10	1	B_2^+	9	1	B_2^-	106456.2	0.38
2	1	A_2^-	1	1	A_2^+	8756.58	−0.15
3	1	B_2^+	2	1	B_2^-	21189.82	−0.13
4	1	A_2^-	3	1	A_2^+	33594.83	−0.09
5	1	B_2^+	4	1	B_2^-	45978.83	−0.13
6	1	A_2^-	5	1	A_2^+	58349.3	0.53
7	1	B_2^+	6	1	B_2^-	70708.9	−0.27
8	1	A_2^-	7	1	A_2^+	83062.95	−0.05
9	1	B_2^+	8	1	B_2^-	95411.5	−0.06
10	1	A_2^-	9	1	A_2^+	107755.2	0.16
4	2	A_2^+	5	1	A_2^-	610301.8	−1.71
3	2	B_2^-	4	1	B_2^+	622426.4	−1.77
2	2	A_2^+	3	1	A_2^-	634590	−2
2	2	B_2^-	2	1	B_2^+	671414.8	1.15
3	2	A_2^+	3	1	A_2^-	671519.8	1.28
4	2	B_2^-	4	1	B_2^+	671659.4	1.17
5	2	A_2^+	5	1	A_2^-	671832.6	−0.08
6	2	B_2^-	6	1	B_2^+	672042.4	0.66
2	2	A_2^+	1	1	A_2^-	695963.1	−0.16
3	2	B_2^-	2	1	B_2^+	708339.2	−0.73
4	2	A_2^+	3	1	A_2^-	720749.1	1.32
5	2	B_2^-	4	1	B_2^+	733185.6	0.22
6	2	A_2^+	5	1	A_2^-	745652.1	0.82
9	2	B_2^-	8	1	B_2^+	783204.9	1.87
4	2	B_2^-	5	1	B_2^+	607247.3	−1.49
2	2	B_2^-	3	1	B_2^+	633305.1	−0.1
2	2	A_2^+	2	1	A_2^-	670757.1	−0.06
3	2	B_2^-	3	1	B_2^+	670232.4	0.92
4	2	A_2^+	4	1	A_2^-	669565.3	0.87
5	2	B_2^-	5	1	B_2^+	668777.2	1.26
6	2	A_2^+	6	1	A_2^-	667883.5	−0.63
7	2	B_2^-	7	1	B_2^+	666904.4	0
2	2	B_2^-	1	1	B_2^+	695741.2	−0.11

(*continued*)

Table 2b. Continued.

J'	K_a'	Γ"	J'	K_a'	Γ′	Frequency	Residual
3	2	A_2^+	2	1	A_2^-	707684	0.32
4	2	B_2^-	3	1	B_2^+	719463	1.46
5	2	A_2^+	4	1	A_2^-	731095	1.41
6	2	B_2^-	5	1	B_2^+	742598.5	−0.27
8	2	B_2^-	7	1	B_2^+	765293.9	−0.53
2	2	E_2^-	2	1	E_2^+	660538	−0.66
3	2	E_2^+	3	1	E_2^-	660648.3	0.68
4	2	E_2^-	4	1	E_2^+	660793.4	0.71
5	2	E_2^+	5	1	E_2^-	660973.7	0.01
6	2	E_2^-	6	1	E_2^+	661190.4	0
7	2	E_2^+	7	1	E_2^-	661442.3	−0.25
8	2	E_2^-	8	1	E_2^+	661729.7	−0.12
2	2	E_2^+	1	1	E_2^-	685087.1	0.03
3	2	E_2^-	2	1	E_2^+	697466.8	−0.41
9	2	E_2^-	8	1	E_2^+	772371.5	0
2	2	E_2^+	2	1	E_2^-	659778.9	0.06
3	2	E_2^-	3	1	E_2^+	659178.7	−0.54
4	2	E_2^+	4	1	E_2^-	658440.1	−0.08
5	2	E_2^-	5	1	E_2^+	657590.8	0.6
6	2	E_2^+	6	1	E_2^-	656652.2	0.52
7	2	E_2^-	7	1	E_2^+	655640.8	−0.47
8	2	E_2^+	8	1	E_2^-	654570.9	−0.15
2	2	E_2^-	1	1	E_2^+	684827	−0.22
3	2	E_2^+	2	1	E_2^-	696708	0.29
2	2	B_2^+	3	1	B_2^-	607318	−0.82
2	2	A_2^-	2	1	A_2^+	644133.3	−1.03
3	2	B_2^+	3	1	B_2^-	644253	−1.03
4	2	A_2^-	4	1	A_2^+	644412.4	−1.15
5	2	B_2^+	5	1	B_2^-	644611.4	−1.43
2	2	B_2^+	1	1	B_2^-	668681.7	1.85
3	2	A_2^-	2	1	A_2^+	681070	0.78
4	2	B_2^+	3	1	B_2^-	693494.4	−0.22
5	2	A_2^-	4	1	A_2^+	705953.9	−0.72
6	2	B_2^+	5	1	B_2^-	718448.9	1.19
7	2	A_2^-	6	1	A_2^+	730972.8	0.47
8	2	B_2^+	7	1	B_2^-	743526.1	−0.74
3	2	B_2^+	4	1	B_2^-	592927.3	−0.73
8	2	B_2^+	8	1	B_2^-	638504.6	−0.64
7	2	A_2^-	7	1	A_2^+	639522.6	0.36
6	2	B_2^+	6	1	B_2^-	640478.9	−1.91
5	2	A_2^-	5	1	A_2^+	641367	−1.46
2	2	B_2^+	2	1	B_2^-	643415.8	−0.75
3	2	A_2^-	3	1	A_2^+	642859.2	−0.77
4	2	B_2^+	4	1	B_2^-	642167.6	−1.02
5	2	A_2^-	5	1	A_2^+	641367	−1.46
2	2	A_2^-	1	1	A_2^+	668437.5	2.11
3	2	B_2^+	2	1	B_2^-	680351.9	0.14
4	2	A_2^-	3	1	A_2^+	692100.3	−1.3
5	2	B_2^+	4	1	B_2^-	703712.5	0.21
6	2	A_2^-	5	1	A_2^+	715212.8	4.01
7	2	B_2^+	6	1	B_2^-	726612.7	1.18
8	2	A_2^-	7	1	A_2^+	737936	−0.19
4	2	A_2^+	3	2	A_2^-	60299.3	−0.08
5	2	B_2^-	4	2	B_2^+	72584.19	−2.09

Table 2b. Continued.

J'	K_a'	Γ"	J'	K_a'	Γ′	Frequency	Residual
6	2	A_2^+	5	2	A_2^-	84863.2	−1.24
7	2	B_2^-	6	2	B_2^+	97131.8	−0.96
8	2	A_2^+	7	2	A_2^-	109388.4	−1.75
4	2	B_2^-	3	2	B_2^+	60299.3	−0.43
5	2	A_2^+	4	2	A_2^-	72585.49	−1.42
6	2	B_2^-	5	2	B_2^+	84864.8	−0.65
7	2	A_2^+	6	2	A_2^-	97134	−0.2
8	2	B_2^-	7	2	B_2^+	109391.6	−0.47
3	2	E_2^+	2	2	E_2^-	36928.57	−0.25
4	2	E_2^-	3	2	E_2^+	49232.47	−0.46
5	2	E_2^+	4	2	E_2^-	61532	−0.31
6	2	E_2^-	5	2	E_2^+	73825.84	0.03
7	2	E_2^+	6	2	E_2^-	86112.2	−0.02
8	2	E_2^-	7	2	E_2^+	98390.4	0.01
9	2	E_2^+	8	2	E_2^-	110659.4	0.28
3	2	E_2^-	2	2	E_2^+	36928.57	−0.04
4	2	E_2^+	3	2	E_2^-	49232.47	0.07
5	2	E_2^-	4	2	E_2^+	61532	0.74
6	2	E_2^+	5	2	E_2^-	73824.04	0.08
7	2	E_2^-	6	2	E_2^+	86109.2	−0.06
8	2	E_2^+	7	2	E_2^-	98386	0.05
9	2	E_2^-	8	2	E_2^+	110653.1	0.32
3	2	E_2^+	3	2	E_2^-	0.26	0
4	2	E_2^-	4	2	E_2^+	0.8	0.01
5	2	E_2^+	5	2	E_2^-	1.88	0.03
6	2	E_2^-	6	2	E_2^+	3.76	0.06
7	2	E_2^+	7	2	E_2^-	6.72	0.06
8	2	E_2^-	8	2	E_2^+	11.2	0.1
9	2	E_2^+	9	2	E_2^-	17.52	0.08
10	2	E_2^-	10	2	E_2^+	26.2	0.04
11	2	E_2^+	11	2	E_2^-	37.71	−0.08
6	2	B_2^+	5	2	B_2^-	62792.3	0.03
7	2	A_2^-	6	2	A_2^+	75096	−0.43
8	2	B_2^+	7	2	B_2^-	87393.8	−0.65
9	2	A_2^-	8	2	A_2^+	99684.8	−0.16
10	2	B_2^+	9	2	B_2^-	111967.1	0.53
6	2	A_2^-	5	2	A_2^+	62792.3	−2.19
7	2	B_2^+	6	2	B_2^-	75099.8	−0.35
8	2	A_2^-	7	2	A_2^+	87399.6	−0.68
9	2	B_2^+	8	2	B_2^-	99693.2	−0.44
10	2	A_2^-	9	2	A_2^+	111979.1	0.13
1	0	A_1^-	0	0	A_1^+	34871.38	−0.06
3	0	A_1^-	2	0	A_1^+	59465.85	−0.08
5	0	A_1^-	4	0	A_1^+	84001.35	−0.29
7	0	A_1^-	6	0	A_1^+	108469.6	−0.19
1	0	E_1^-	0	0	E_1^+	12321	−0.01
2	0	E_1^+	1	0	E_1^-	24640.81	0
3	0	E_1^-	2	0	E_1^+	36958.13	−0.08
4	0	E_1^+	3	0	E_1^-	49271.94	−0.08
5	0	E_1^-	4	0	E_1^+	61581.12	0.1
6	0	E_1^+	5	0	E_1^-	73884	−0.03
7	0	E_1^-	6	0	E_1^+	86179.95	0.1
8	0	E_1^+	7	0	E_1^-	98467	−0.27
9	0	E_1^-	8	0	E_1^+	110745	−0.09

(*continued*)

Table 2b. Continued.

J'	$K_a^{`}$	Γ'	J''	K_a''	Γ''	Frequency	Residual
2	0	A_1^+	1	0	A_1^-	2110.36	0.09
4	0	A_1^+	3	0	A_1^-	26810.57	−0.03
6	0	A_1^+	5	0	A_1^-	51535.65	−0.16
8	0	A_1^+	7	0	A_1^-	76275.3	−0.05
10	0	A_1^+	9	0	A_1^-	101018.2	−0.04
3	1	A_1^-	4	0	A_1^+	404054.9	−0.17
1	1	A_1^-	2	0	A_1^+	428731.67	0.04
2	1	A_1^-	2	0	A_1^+	453392	−0.26
4	1	A_1^-	4	0	A_1^+	453392.8	−0.09
6	1	A_1^-	6	0	A_1^+	453395.3	0.21
8	1	A_1^-	8	0	A_1^+	453400.3	−0.18
1	1	A_1^-	0	0	A_1^+	465713.34	0
3	1	A_1^-	2	0	A_1^+	490332	0.41
5	1	A_1^-	4	0	A_1^+	514910.9	0.54
7	1	A_1^-	6	0	A_1^+	539441.2	−0.07
4	1	E_1^+	5	0	E_1^-	367308.53	−0.47
3	1	E_1^-	4	0	E_1^+	379590.38	−0.26
2	1	E_1^+	3	0	E_1^-	391883.86	−0.09
1	1	E_1^-	2	0	E_1^+	404187.79	0.08
1	1	E_1^+	1	0	E_1^-	428833.58	0.04
2	1	E_1^-	2	0	E_1^+	428857.38	0.15
3	1	E_1^+	3	0	E_1^-	428892.98	0.19
4	1	E_1^-	4	0	E_1^+	428940.45	0.2
5	1	E_1^+	5	0	E_1^-	428999.9	0.23
6	1	E_1^-	6	0	E_1^+	429071.26	0.18
7	1	E_1^+	7	0	E_1^-	429154.64	0.07
8	1	E_1^-	8	0	E_1^+	429250.17	−0.04
9	1	E_1^+	9	0	E_1^-	429357.75	−0.33
1	1	E_1^-	0	0	E_1^+	441149.58	0.06
2	1	E_1^+	1	0	E_1^-	453482.93	−0.03
3	1	E_1^-	2	0	E_1^+	465820.5	−0.36
4	1	E_1^+	3	0	E_1^-	478162.3	0.26
5	1	E_1^-	4	0	E_1^+	490505.2	−0.15
6	1	E_1^+	5	0	E_1^-	502849.7	0.06
7	1	E_1^-	6	0	E_1^+	515193.4	−0.39
8	1	E_1^+	7	0	E_1^-	527536.9	0.24
9	1	E_1^-	8	0	E_1^+	539877.5	0.35
2	1	A_1^+	3	0	A_1^-	372784.99	−0.09
1	1	A_1^+	1	0	A_1^-	409708.1	0.1
3	1	A_1^+	3	0	A_1^-	409815.62	0.16
5	1	A_1^+	5	0	A_1^-	410008.91	0.28
7	1	A_1^+	7	0	A_1^-	410287.2	0.09
2	1	A_1^+	1	0	A_1^-	434361.24	−0.03
4	1	A_1^+	3	0	A_1^-	459083.49	−0.42
6	1	A_1^+	5	0	A_1^-	483844.2	−0.39
8	1	A_1^+	7	0	A_1^-	508633.2	−0.12
5	1	A_1^-	4	1	A_1^+	82637.25	0.2
7	1	A_1^-	6	1	A_1^+	107133	0.51
4	1	A_1^-	3	1	A_1^+	70387.7	−0.33
6	1	A_1^-	5	1	A_1^+	94922	−0.27
2	1	E_1^+	1	1	E_1^-	24654.34	−0.1
3	1	E_1^-	2	1	E_1^+	36978.5	−0.2
4	1	E_1^+	3	1	E_1^-	49299.16	−0.23
5	1	E_1^-	4	1	E_1^+	61615.26	−0.06

Table 2b. Continued.

J'	$K_a^{`}$	Γ'	J''	K_a''	Γ''	Frequency	Residual
6	1	E_1^+	5	1	E_1^-	73925.5	0.18
7	1	E_1^-	6	1	E_1^+	86228.05	−0.13
8	1	E_1^+	7	1	E_1^-	98522.8	0.08
9	1	E_1^-	8	1	E_1^+	110808.2	0.44
2	1	E_1^-	1	1	E_1^+	24664.55	0.06
3	1	E_1^+	2	1	E_1^-	36993.72	−0.05
4	1	E_1^-	3	1	E_1^+	49319.49	0.01
5	1	E_1^+	4	1	E_1^-	61640.54	0.1
6	1	E_1^-	5	1	E_1^+	73955.7	0.25
7	1	E_1^+	6	1	E_1^-	86263.2	−0.14
8	1	E_1^-	7	1	E_1^+	98562.6	−0.3
9	1	E_1^+	8	1	E_1^-	110852.48	−0.48
8	1	A_1^+	7	1	A_1^-	77661.6	−0.24
10	1	A_1^+	9	1	A_1^-	102386	0.7
7	1	A_1^+	6	1	A_1^-	65362.4	0.59
9	1	A_1^+	8	1	A_1^-	90111.6	−0.14
11	1	A_1^+	10	1	A_1^-	114855.8	−0.36
1	1	E_1^+	1	1	E_1^-	5.1	0.07
2	1	E_1^-	2	1	E_1^+	15.3	0.23
3	1	E_1^+	3	1	E_1^-	30.54	0.41
4	1	E_1^-	4	1	E_1^+	50.82	0.59
6	2	A_1^-	5	2	A_1^+	85847.7	−0.4
8	2	A_1^-	7	2	A_1^+	110322.8	0.12
5	2	A_1^-	4	2	A_1^+	73598.3	0.36
7	2	A_1^-	6	2	A_1^+	98089.4	−0.05
3	2	E_1^+	2	2	E_1^-	36863.51	0.05
4	2	E_1^-	3	2	E_1^+	49146.13	0.13
6	2	E_1^-	5	2	E_1^+	73697.04	0.7
7	2	E_1^+	6	2	E_1^-	85962.7	0.82
8	2	E_1^-	7	2	E_1^+	98221	1.51
9	2	E_1^+	8	2	E_1^-	110469.4	1.37
3	2	E_1^-	2	2	E_1^+	36863.51	−0.11
4	2	E_1^+	3	2	E_1^-	49146.13	−0.25
6	2	E_1^+	5	2	E_1^-	73697.04	−0.62
7	2	E_1^-	6	2	E_1^+	85963.35	−0.64
8	2	E_1^+	7	2	E_1^-	98221	−1.66
9	2	E_1^-	8	2	E_1^+	110471.2	−1.37
3	2	E_1^-	3	2	E_1^+	0.51	0.32
4	2	E_1^+	4	2	E_1^-	0.98	0.41
5	2	E_1^-	5	2	E_1^+	1.76	0.44
6	2	E_1^+	6	2	E_1^-	2.88	0.23
7	2	E_1^-	7	2	E_1^+	4.5	−0.26
8	2	E_1^+	8	2	E_1^-	9.64	1.7
7	2	A_1^+	6	2	A_1^-	73834.96	0.33
9	2	A_1^+	8	2	A_1^-	98403.2	−0.12
8	2	A_1^+	7	2	A_1^-	86123	−0.32
10	2	A_1^+	9	2	A_1^-	110676.6	0.14

Γ: symmetry species of the level in the molecular symmetry group G_{16}.
RMS: 0.621 MHz.
Negative values indicate only lower relative frequencies and not emissions for $(H_2O)_2$.

Appendix B

Table 4. Fingerprint of $E_2 \leftrightarrow E_1$ transitions for $(H_2O)_2$ and $(D_2O)_2$ in (MHz).

	$(H_2O)_2$	$(D_2O)_2$
$E_i\,(J,\,K_a) \rightarrow E_f\,(J,\,K_a)$	Relative frequency	Relative frequency
$E_2^+\,(1,0) \rightarrow E_1^-\,(1,1)$	−149299.21	77520.03
$E_2^-\,(2,0) \rightarrow E_1^+\,(2,1)$	−149669.29	77555.35
$E_2^+\,(3,0) \rightarrow E_1^-\,(3,1)$	−150183.00	77608.31
$E_2^-\,(4,0) \rightarrow E_1^+\,(4,1)$	−150807.17	77678.93
$E_2^+\,(5,0) \rightarrow E_1^-\,(5,1)$	−151512.91	77767.2
$E_2^-\,(6,0) \rightarrow E_1^+\,(6,1)$	−152277.44	77873.12
$E_2^+\,(7,0) \rightarrow E_1^-\,(7,1)$	−153083.63	77996.69
$E_2^-\,(8,0) \rightarrow E_1^+\,(8,1)$	−153918.82	78137.89
$E_2^+\,(9,0) \rightarrow E_1^-\,(9,1)$	−154773.69	78296.74
$E_2^-\,(10,0) \rightarrow E_1^+\,(10,1)$	−155641.31	78473.21
$E_2^+\,(11,0) \rightarrow E_1^-\,(11,1)$	−156516.52	78667.32
$E_2^-\,(12,0) \rightarrow E_1^+\,(12,1)$	−157395.42	78879.05
$E_2^-\,(0,0) \rightarrow E_1^+\,(1,1)$	−161437.05	88351.5
$E_2^+\,(1,0) \rightarrow E_1^-\,(2,1)$	−173968.72	99184.4
$E_2^-\,(2,0) \rightarrow E_1^+\,(3,1)$	−186678.13	110000.1
$E_2^+\,(3,0) \rightarrow E_1^-\,(4,1)$	−199532.61	120797.7
$E_2^-\,(4,0) \rightarrow E_1^+\,(5,1)$	−212497.83	131576.5
$E_2^+\,(5,0) \rightarrow E_1^-\,(6,1)$	−225543.7	142335.6
$E_2^-\,(6,0) \rightarrow E_1^+\,(7,1)$	−238646.25	153074
$E_2^+\,(7,0) \rightarrow E_1^-\,(8,1)$	−251787.15	163791
$E_2^-\,(8,0) \rightarrow E_1^+\,(9,1)$	−264952.58	174485.7
$E_2^+\,(9,0) \rightarrow E_1^-\,(10,1)$	−278132.01	185157.3
$E_2^-\,(2,0) \rightarrow E_1^+\,(1,1)$	−125019.86	55758.53
$E_2^+\,(3,0) \rightarrow E_1^-\,(2,1)$	−113219.36	44865.56
$E_2^-\,(4,0) \rightarrow E_1^+\,(3,1)$	−101537.91	33959.69
$E_2^+\,(5,0) \rightarrow E_1^-\,(4,1)$	−89947.81	23041.77
$E_2^-\,(6,0) \rightarrow E_1^+\,(5,1)$	−78427.47	12112.67
$E_2^+\,(7,0) \rightarrow E_1^-\,(6,1)$	−66960.93	1173.22
$E_2^-\,(8,0) \rightarrow E_1^+\,(7,1)$	−55536.73	−9775.71
$E_2^+\,(9,0) \rightarrow E_1^-\,(8,1)$	−44146.74	−20733.3
$E_2^-\,(10,0) \rightarrow E_1^+\,(9,1)$	−32785.23	−31698.6
$E_2^-\,(1,1) \rightarrow E_1^+\,(1,1)$	−138002.75	−6185.86
$E_2^+\,(2,1) \rightarrow E_1^-\,(2,1)$	−138118.78	−6149.76
$E_2^-\,(3,1) \rightarrow E_1^+\,(3,1)$	−138292.69	−6095.62
$E_2^+\,(4,1) \rightarrow E_1^-\,(4,1)$	−138524.31	−6023.44
$E_2^-\,(5,1) \rightarrow E_1^+\,(5,1)$	−138813.43	−5933.22
$E_2^+\,(6,1) \rightarrow E_1^-\,(6,1)$	−139159.79	−5824.99
$E_2^-\,(7,1) \rightarrow E_1^+\,(7,1)$	−139563.04	−5698.76
$E_2^+\,(8,1) \rightarrow E_1^-\,(8,1)$	−140022.82	−5554.54
$E_2^-\,(9,1) \rightarrow E_1^+\,(9,1)$	−140538.68	−5392.35
$E_2^-\,(1,1) \rightarrow E_1^+\,(2,1)$	−162652.18	−40358
$E_2^+\,(2,1) \rightarrow E_1^-\,(3,1)$	−175082.42	−51340
$E_2^-\,(3,1) \rightarrow E_1^+\,(4,1)$	−187561.94	−62370.6
$E_2^+\,(4,1) \rightarrow E_1^-\,(5,1)$	−200089.41	−73449
$E_2^-\,(5,1) \rightarrow E_1^+\,(6,1)$	−212663.41	−84574.2
$E_2^+\,(6,1) \rightarrow E_1^-\,(7,1)$	−225282.49	−95745.5
$E_2^-\,(7,1) \rightarrow E_1^+\,(8,1)$	−237945.13	−106962
$E_2^+\,(8,1) \rightarrow E_1^-\,(9,1)$	−250649.76	−118222
$E_2^-\,(9,1) \rightarrow E_1^+\,(10,1)$	−263394.76	−129526
$E_2^+\,(2,1) \rightarrow E_1^-\,(1,1)$	−113449.27	−27814.1
$E_2^-\,(3,1) \rightarrow E_1^+\,(2,1)$	−101283.85	−38540.4
$E_2^+\,(4,1) \rightarrow E_1^-\,(3,1)$	−89174.70	−49212.9
$E_2^-\,(5,1) \rightarrow E_1^+\,(4,1)$	−77122.78	−59830.8
$E_2^+\,(6,1) \rightarrow E_1^-\,(5,1)$	−65129.00	−70393.4
$E_2^-\,(7,1) \rightarrow E_1^+\,(6,1)$	−53194.24	−80899.7
$E_2^+\,(8,1) \rightarrow E_1^-\,(7,1)$	−41319.29	−91348.9
$E_2^-\,(9,1) \rightarrow E_1^+\,(8,1)$	−29504.92	−101740
$E_2^+\,(10,1) \rightarrow E_1^-\,(9,1)$	−17751.83	−112073
$E_2^+\,(1,1) \rightarrow E_1^-\,(1,1)$	−137737.83	−18534.7
$E_2^-\,(2,1) \rightarrow E_1^+\,(2,1)$	−137343.95	−18518
$E_2^+\,(3,1) \rightarrow E_1^-\,(3,1)$	−136794.45	−18492.9
$E_2^-\,(4,1) \rightarrow E_1^+\,(4,1)$	−136122.37	−18459.4
$E_2^+\,(5,1) \rightarrow E_1^-\,(5,1)$	−135356.46	−18417.5
$E_2^-\,(6,1) \rightarrow E_1^+\,(6,1)$	−134519.30	−18367.2
$E_2^+\,(7,1) \rightarrow E_1^-\,(7,1)$	−133627.80	−18308.5
$E_2^-\,(8,1) \rightarrow E_1^+\,(8,1)$	−132694.34	−18241.4
$E_2^+\,(9,1) \rightarrow E_1^-\,(9,1)$	−131727.94	−18165.8
$E_2^+\,(1,1) \rightarrow E_1^-\,(2,1)$	−162407.35	−40199.1
$E_2^-\,(2,1) \rightarrow E_1^+\,(3,1)$	−174352.79	−50962.7
$E_2^+\,(3,1) \rightarrow E_1^-\,(4,1)$	−186144.06	−61682.3
$E_2^-\,(4,1) \rightarrow E_1^+\,(5,1)$	−197813.03	−72357
$E_2^+\,(5,1) \rightarrow E_1^-\,(6,1)$	−209387.24	−82985.9
$E_2^-\,(6,1) \rightarrow E_1^+\,(7,1)$	−220888.10	−93568.1
$E_2^+\,(7,1) \rightarrow E_1^-\,(8,1)$	−232331.32	−104103
$E_2^-\,(8,1) \rightarrow E_1^+\,(9,1)$	−243728.10	−114589
$E_2^+\,(9,1) \rightarrow E_1^-\,(10,1)$	−255086.26	−125026
$E_2^-\,(2,1) \rightarrow E_1^+\,(1,1)$	−112694.52	3278.84
$E_2^+\,(3,1) \rightarrow E_1^-\,(2,1)$	−99830.81	14249.89
$E_2^-\,(4,1) \rightarrow E_1^+\,(3,1)$	−86853.12	25259.87
$E_2^+\,(5,1) \rightarrow E_1^-\,(4,1)$	−73791.36	36307.94
$E_2^-\,(6,1) \rightarrow E_1^+\,(5,1)$	−60669.32	47393.25
$E_2^+\,(7,1) \rightarrow E_1^-\,(6,1)$	−47505.09	58514.95
$E_2^-\,(8,1) \rightarrow E_1^+\,(7,1)$	−34312.25	69672.22
$E_2^+\,(9,1) \rightarrow E_1^-\,(8,1)$	−21101.00	80864.22
$E_2^-\,(10,1) \rightarrow E_1^+\,(9,1)$	−7879.090	92090.1
$E_2^+\,(1,1) \rightarrow E_1^-\,(1,0)$	291090.67	136732.5
$E_2^-\,(2,1) \rightarrow E_1^+\,(2,0)$	291498.20	136784.8
$E_2^+\,(3,1) \rightarrow E_1^-\,(3,0)$	292068.19	136863.2
$E_2^-\,(4,1) \rightarrow E_1^+\,(4,0)$	292767.64	136967.9
$E_2^+\,(5,1) \rightarrow E_1^-\,(5,0)$	293567.86	137098.9
$E_2^-\,(6,1) \rightarrow E_1^+\,(6,0)$	294446.30	137256.4
$E_2^+\,(7,1) \rightarrow E_1^-\,(7,0)$	295386.13	137440.4
$E_2^-\,(8,1) \rightarrow E_1^+\,(8,0)$	296375.05	137651.1
$E_2^+\,(9,1) \rightarrow E_1^-\,(9,0)$	297404.12	137888.6
$E_2^+\,(1,1) \rightarrow E_1^-\,(2,0)$	266189.97	114944.8
$E_2^-\,(2,1) \rightarrow E_1^+\,(3,0)$	253780.22	104016.1
$E_2^+\,(3,1) \rightarrow E_1^-\,(4,0)$	241328.07	93056.65
$E_2^-\,(4,1) \rightarrow E_1^+\,(5,0)$	228834.90	82067.41
$E_2^+\,(5,1) \rightarrow E_1^-\,(6,0)$	216302.19	71049.34
$E_2^-\,(6,1) \rightarrow E_1^+\,(7,0)$	203731.44	60003.4
$E_2^+\,(7,1) \rightarrow E_1^-\,(8,0)$	191124.26	48930.59

(*continued*)

Table 4. Continued.

	$(H_2O)_2$	$(D_2O)_2$
$E_2^-(8,1) \rightarrow E_1^+(9,0)$	178482.3	37831.93
$E_2^+(9,1) \rightarrow E_1^-(10,0)$	165807.28	26708.45
$E_2^+(1,1) \rightarrow E_1^-(0,0)$	303151.78	147537.5
$E_2^-(2,1) \rightarrow E_1^+(1,0)$	315379.24	158334.4
$E_2^+(3,1) \rightarrow E_1^-(2,0)$	327558.3	169096.1
$E_2^-(4,1) \rightarrow E_1^+(3,0)$	339687.94	179822
$E_2^+(5,1) \rightarrow E_1^-(4,0)$	351767.24	190511.1
$E_2^-(6,1) \rightarrow E_1^+(5,0)$	363795.32	201162.8
$E_2^+(7,1) \rightarrow E_1^-(6,0)$	375771.36	211776.2
$E_2^-(8,1) \rightarrow E_1^+(7,0)$	387694.64	222350.8
$E_2^+(9,1) \rightarrow E_1^-(8,0)$	399564.46	232885.6
$E_2^-(10,1) \rightarrow E_1^+(9,0)$	411380.23	243380.1

References

[1] F. N. Keutsch and R. J. Saykally, PNAS **98**(19), 10533–10540 (2000).
[2] M. P. Hodges, A. J. Stone, and S. S. Xantheas, J. Phys. Chem. **101,** 9163–9168 (1997).
[3] E. M. Mas and J. Szalewicz, J. Chem. Phys. **104,** 7606–7614 (1996).
[4] N. Goldman and R. J. Saykally, J. Chem. Phys. **120,** 4777–4789 (2004).
[5] E. M. Mas, R. Bukowski, S. K., G. C. Groenenboom, P. E. S. Wormer, and A. v. d. Avoird, J. Chem. Phys. **113,** 6687–6701 (2000).
[6] C. Leforestier, F. Gatti, R. S. Fellers, and R. J. Saykally, J. Chem. Phys. **117,** 8710–8722 (2002).
[7] J. B. Paul and R. J. Saykally, J. Phys. Chem. **102,** 3279–3283 (1998).
[8] T. R. Dyke and J. S. Muenter, J. Chem. Phys. **60,** 2929–2930 (1974).
[9] T. R. Dyke, J. Chem. Phys. **66,** 492–497 (1977).
[10] T. R. Dyke, K. M. Mack, and J. S. Muenter, J. Chem. Phys. **66,** 498–510 (1977).
[11] J. T. Hougen, J. Mol. Spectrosc. **114**(2), 395–426 (1985).
[12] L. H. Coudert and J. T. Hougen, J. Mol. Spectrosc. **130,** 86–119 (1988).
[13] G. T. Fraser, Int. Rev. Phys. Chem. **10,** 189 (1991).
[14] L. B. Braly, J. D. Cruzan, K. Liu, R. S. Fellers, and R. J. Saykally, J. Chem. Phys. **112**(23), 10314–10326 (2000).
[15] L. B. Braly, K. Liu, M. G. Brown, F. N. Keutsch, R. S. Fellers, and R. J. Saykally, J. Chem. Phys. **112**(23), 10293–10313 (2000).
[16] L. H. Coudert and J. T. Hougen, J. Mol. Spectrosc. **139,** 259 (1990).
[17] D. J. Wales, Adv. Mol. Vibrat. Collision Dynam. **3,** 365–2000 (1998).
[18] R. S. Fellers, C. Leforestier, L. B. Braly, M. G. Brown, and R. J. Saykally, Science **284,** 945 (1999).
[19] T. Taketsugu and D. J. Wales, Mol. Phys. **100**(17), 2793–2806 (2002).
[20] G. S. Tschumper, B. C. Hoffman, E. F. Valeev, H. F. Schaefer III, and M. Quack, J. Chem. Phys. **116**(2), 690–701 (2002).
[21] Y. Watanabe, T. Taketsugufoot, and D. J. Wales, J. Chem. Phys. **120**(13), 5993–5999 (2004).
[22] G. T. Fraser, L. H. Suenram, and L. H. Coudert, J. Chem. Phys. **90,** 6077 (1989).
[23] F. N. Keutsch, *Chemistry* (University of California, Berkeley, 2001).
[24] M. J. Smit, G. C. Groenenboom, P. E. S. Wormer, and A. v. d. Avoird, J. Phys. Chem. **105,** 6212 (2001).
[25] C. Leforestier, and Y. Scribano. Personal communication (2004).
[26] E. N. Karyakin, G. T. Fraser, and L. H. Suenram, Mol. Phys. **78,** 1179 (1993).
[27] F. N. Keutsch, N. Goldman, E. N. Karyakin, H. A. Harker, M. E. Sanz, C. Leforestier, and R. J. Saykally, Faraday Discussions **118,** 79–93 (2001).
[28] F. N. Keutsch, L. B. Braly, M. G. Brown, H. A. Harker, P. B. Petersen, C. Leforestier, and R. J. Saykally, J. Chem. Phys. **119**(17), 8927–8937 (2003).
[29] L. A. Surin, Rev. Sci. Instrum. **72,** 2535 (2001).
[30] L. H. Suenram, G. T. Fraser, and F. J. Lovas, J. Mol. Spectrosc. **138,** 440 (1989).
[31] E. Zwart, J. J. ter Meulen, and W. L. Meerts, Chem. Phys. Lett. **173,** 115 (1990).
[32] E. Zwart, J. J. ter Meulen, W. L. Meerts, and L. H. Coudert, J. Mol. Spectrosc. **147,** 27 (1991).
[33] E. Zwart, J. J. ter Meulen, and W. L. Meerts, Chem. Phys. Lett. **166,** 500 (1990).
[34] T. A. Hu and T. R. Dyke, J. Chem. Phys. **91,** 7348 (1989).
[35] K. L. Busarow, R. C. Cohen, G. A. Blake, K. B. Laughlin, Y. T. Lee, and R. J. Saykally, J. Chem. Phys. **90**(8), 3937–3943 (1989).
[36] J. A. Odutola, T. A. Hu, D. Prinslow, S. E. O'dell, and T. R. Dyke, J. Chem. Phys. **88,** 5352 (1988).
[37] G. T. Fraser, L. H. Suenram, L. H. Coudert, and R. S. Frye, J. Mol. Spectrosc. **137,** 244 (1989).
[38] L. H. Coudert, F. J. Lovas, L. H. Suenram, and J. T. Hougen, J. Chem. Phys. **87,** 6290 (1987).
[39] F. N. Keutsch, N. Goldman, H. A. Harker, C. Leforestier, and R. J. Saykally, Mol. Phys. **101**(23–24), 3477–3492 (2003).